

REAL-TIME SIMULATION OF SHIPBOARD POWER SYSTEM
AND ENERGY STORAGE DEVICE MANAGEMENT

by

DINGYI LI

B.S., Kansas State University, 2012

A THESIS

submitted in partial fulfillment of the requirements for the degree

MASTER OF SCIENCE

Department of Electrical and Computer Engineering
College of Engineering

KANSAS STATE UNIVERSITY
Manhattan, Kansas

2014

Approved by:

Major Professor
Dr. Noel Schulz

Abstract

Many situations can cause a fault on a shipboard power system, especially in naval battleships. Batteries and ultra-capacitors are simulated to be backup energy storage devices (ESDs) to power the shipboard power system when an outage or damage occurs. Because ESDs have advantages such as guaranteed load leveling, good transient operation, and energy recovery during braking operation, they are commonly used for electrical ship applications. To fulfill these requirements, an energy management subsystem (EMS) with a specific control algorithm must connect ESDs to the dc link of the motor drive system. In this research, the real-time simulation of shipboard power system (SPS), bidirectional DC-DC converter, EMS, and ESDs are designed, implemented, and controlled on OPAL-RT system to test SPS survivability and ESD performance in various speed operations.

Table of Contents

List of Figures	v
List of Tables	vii
Acknowledgements	viii
Chapter 1 - Introduction.....	1
1.1 Shipboard Power System	1
1.2 Energy Storage Devices.....	2
1.3 Energy Management Subsystem.....	2
1.4 Thesis Objective	3
Chapter 2 - Review of Related Works	5
2.1 Shipboard Power System	5
2.2 Energy Storage Device	6
2.3 Real Time Simulation	6
2.3.1 Introduction of Real Time Simulation	6
2.3.2 Function of Real-time simulation	7
2.3.3 RT-LAB for Real Time Simulation	8
2.4 Conclusion	10
Chapter 3 - Models of the Shipboard Power System.....	11
3.1 Corzine Model of the Shipboard Power System.....	11
3.2 Simplified Model of the Shipboard Power System	12
3.2.1 Simulation of Generators	13
3.2.2 Simulation of Motor.....	15
3.2.3 Simulation of AC Loads	16
3.2.4 Simulation of Constant Power Load	17
Chapter 4 - Modes of Energy Storage Devices.....	18
4.1 Battery Equivalent Circuit and Simulink Model	18
4.1.1 Electrical Model and Mathematical Equations	19
4.1.2 Simulink Model of the Battery	20
4.2 Ultracapacitor Equivalent Circuit and Simulink Model	23
4.2.1 Electrical Model and Mathematical Equations for Ultracapacitor.....	23

4.2.2 Simulink Model of the Ultracapacitor	25
4.3 Summary	26
Chapter 5 - Model of the Bi-directional DC-DC Converter	27
5.1 Bi-directional DC-DC Converter Control Strategy	27
5.2 Bi-directional DC-DC Converter Matlab Simulink Model	29
5.2.1 Dynamic Analysis of the Bi-directional DC-DC Converter	29
5.2.2 Simulink Models of the Converter	39
5.3 Matlab Simulink Results of the Bi-directional DC-DC Converter	39
Chapter 6 - Energy Management System	40
6.1 Battery Management Subsystem	40
6.2 Power Management Subsystem	41
6.3 Summary	43
Chapter 7 - Performance and Testing of the Developed Models	45
7.1 Stability of Shipboard Power System	45
7.2 Energy Management System Performance	47
Chapter 8 - Discussion and Future Work	51
References	53
Appendix A - Parameters of Battery	55
Appendix B - Figures	60

List of Figures

Figure 2.1 Joseph’s Corzine Model of a Shipboard Power System (adapted from [1])	6
Figure 3.1 Corzine Model of a Shipboard Power System	12
Figure 3.2 Simplified Model of Shipboard Power System	13
Figure 3.3 Simulation Model of Generator	14
Figure 3.4 Simulation of Fault Placement on Generator	14
Figure 3.5 Control Diagram of the Generator Output Voltage	15
Figure 3.6 Simulation of Motor	16
Figure 3.7 Simulation of AC Loads	17
Figure 4.1 Electrical Battery Model [8]	20
Figure 4.2 Electrical Battery Model in Simulink	21
Figure 4.3 SOC Estimation Block[8]	22
Figure 4.4 Component and Terminal Voltage Estimation Block	23
Figure 4.5 Simplified Electric Model for Ultracapacitor [8]	24
Figure 4.6 Mathematical Model for Ultracapacitor[8]	25
Figure 4.7 Simulink Model for Ultracapacitor [11]	26
Figure 5.1 Power Circuit of a Bidirectional DC-DC Converter	28
Figure 5.2 Control Circuit for Bidirectional DC-DC Converter	29
Figure 5.3 Voltages and Currents for Boost and Buck DC-DC Converter	30
Figure 5.4 Interval 1: Voltages and Currents for Boost DC-DC Converter	30
Figure 5.5 Interval 2: Voltages and Currents for Boost DC-DC Converter	31
Figure 5.6 Interval 1: Voltages and Currents for Buck DC-DC Converter	31
Figure 5.7 Interval 2: Voltages and Currents for Buck DC-DC Converter	32
Figure 5.8 Simulink model of the bi-directional DC-DC converter	39
Figure 6.1 Battery Management Subsystem	40
Figure 6.2 Power Management Subsystem	42
Figure 6.3 Battery Available Power Subsystem	42
Figure 7.1 Simulation results in case of a Starboard Fault	46
Figure 7.2 Simulation results of acceleration factor, and power of generator, motor and battery	49
Figure 7.3 Simulation results of PMSM motor drive parameters	49

Figure 7.4 Simulation results of SOC, voltage and current of battery, and voltage and current of generator and DC-DC converter 50

Figure 7.5 Simulation results of drive power, motor power, battery power and generator power 50

Figure 8.1 Diagram of powertrain using designed model..... 52

List of Tables

Table 6.1 Speed vs. Torque for Motor to calculate P_drive	42
Table 7.1 Processor Allocation and Real-Time Performance in case of a Starboard Fault.....	47

Acknowledgements

I would like to thank my academic advisor, Dr. Noel Schulz, for her guidance and support on the path of completing my Master's program. I would also like to thank the other committee members, Dr. Anil Pahwa and Dr. Shelli Starrett, for their guidance.

Special thanks to the United States Office of Naval Research for their financial support through grant N00014-10-1-0431 under the DEPSCoR program.

Finally, I would like to thank my family and friends for their encouragement and support throughout this program and before to get to this point.

Chapter 1 - Introduction

Reliable electrical power has become one of the main necessities in the modern world. Because of the dependence on electrical power, alternative solutions are needed for restoration and recover after an outage or fault on the system. In this case having storage devices within the power system can provide back-up power or power during the transition.

Shipboard power systems present a special set of challenges related to restoration so having effectively integrate Energy Storage Devices (ESD) as part of the system can provide opportunities related to reliability and flexibility operations. An Energy Storage Device Subsystem is an essential element of shipboard power system and of an increasing number of terrestrial electric systems. This element stores a great amount of energy that can be released when necessary. The battery enables regenerative braking in an electric system and allows supplementing other energy source, such as the synchronized machine. It is important that the electric system can be fed by ESDs when the fault is located in the system. If the ESDs cannot provide energy to the system when a fault occurs, electrical equipment and other parts of the system may experience outages or operational issues.

1.1 Shipboard Power System

In this research, the shipboard power systems (SPS) the focus area. The U.S. Navy is looking at the next generation ship, which may include a DC power system with multiple power elements [1]. These power elements include multiple generators, loads and power lines. The

main generators throughout the system generate AC power. This AC power is then converted to DC power by three-level AC-DC bridge converter. A voltage controller works with this converter in order to keep the DC voltage at the required level.

There are many situations that can cause a fault on a shipboard. These situations include being hit by artillery from enemy ships and daily wear in the shipboard system [1]. However, the integration of SPS and the ESDs can highly increase the stability, reliability and survivability of the system when a fault occurs.

1.2 Energy Storage Devices

Electric storage systems are crucial in order to improve quality of service of future electric ships. Batteries and ultra-capacitors are often used to be the backup energy storage devices (ESDs) to power the shipboard power system when an outage and damage happen. The SPS is required to function in three different modes namely: steady-state (normal) mode, acceleration mode (increasing speed of the ship) and braking (regenerative) mode. During acceleration mode the power flow is from ESDs to the SPS whereas during regenerative mode the kinetic energy of the motor is converted into electrical energy and fed back to battery. Also, generators inside of SPS can charge the battery packs under normal mode when the State-Of-Charge (SOC) level of battery packs are below the standard level.

1.3 Energy Management Subsystem

The Energy Management Subsystem (EMS) determines the reference signals for the electric motor drives, the electric generator drive and the ESDs in order to distribute accurately the power from the two electrical sources. These signals are calculated using mainly the acceleration rate of ship, related to movement in the water. The acceleration can reach up to +100% when the motors are in full propulsion mode and can be -100% when the ship is in full braking mode (regenerative) or -100% acceleration rates. The battery management system can be set to keep the State-of-Charge (SOC) of the battery between specified boundaries to work to maximize operational impact as well as minimize battery deterioration.

Also, it prevents against voltage collapse by controlling the power required from the battery. The Power management system controls the reference power of the electrical motor by splitting the power demand as a function of the available power of the battery and the generator. The required generator power is achieved by controlling the generator torque, the motor torque and the battery recharge power.

1.4 Thesis Objective

The objective of this thesis is to develop an energy management system to integrate the backup energy storage device and the shipboard power system. In order to develop the control diagram, shipboard power system and energy storage devices, and bidirectional DC/DC converter need to be modeled and simulated. Each part of the system, the generator, converter, and load, need to be modeled in the selected simulation software. A method must be produced to accurately control the power flow in the system. A novel approach integrating the storage and

power system is used to determine required power in the power system. The torque of the motor, torque of the generator, and battery parameters are used as the input to this management control diagram. The state of charge level of the battery is also controlled by a battery management subsystem. The performances of the SPS, EDSs, bidirectional DC/DC converter and the energy management system are tested and verified in this research. These methods should be able to convert the SPS to electric system with backup energy storage devices. Test cases, such as steady-state (normal) mode, acceleration mode and braking (regenerative) mode, are used to fully test these methods throughout the process.

The contributions of this work include: building the new shipboard power system with detailed loads model which can be fed by the generators in redundantly way. A bidirectional DC-DC converter with output voltage control and power control is designed in this work. Last, a torque-controlled Energy Management System for electrical power system with backup energy storage devices is designed for this research

Chapter 2 - Review of Related Works

The importance of shipboard power system and energy storage devices in this research was discussed in the previous chapter. One of the keys before developing the models and system is to review the previous work that has been done related to shipboard power systems and storage. Joseph Dieker [1] and Amanuel Kesete [8] from Kansas State University have developed the shipboard power system model, battery model, and ultracapacitor model in 2012 to fulfill their master's research study. The following chapter discusses the background research and models that were developed at Kansas State in previous research that provided the start to these research efforts. Additionally some information about other related work is outlined.

2.1 Shipboard Power System

Joseph Dieker, in his thesis titled “High impedance fault identification using Bayesian analysis in a shipboard power system” [1], presented a Corzine shipboard power system model [1]. The total number of generators in this system equals four, with the two distributed generators producing 4 MW and the two main generators operating at 6 MW [1].

This model has five load zones that contain two non-vital loads, one semi-vital load, and one vital load. The generators are connected to the loads using two buses. The loads in the system represent motors, artillery and other equipment in the ship. There are switches that connect the higher priority loads to either the port side or starboard side bus, as seen below in Figure 2.1. The loads on point 35 and 79 are inserted into the model to represent the motors of the SPS. The motors are represented single vital load and are connected to one bus and a generator through switches.

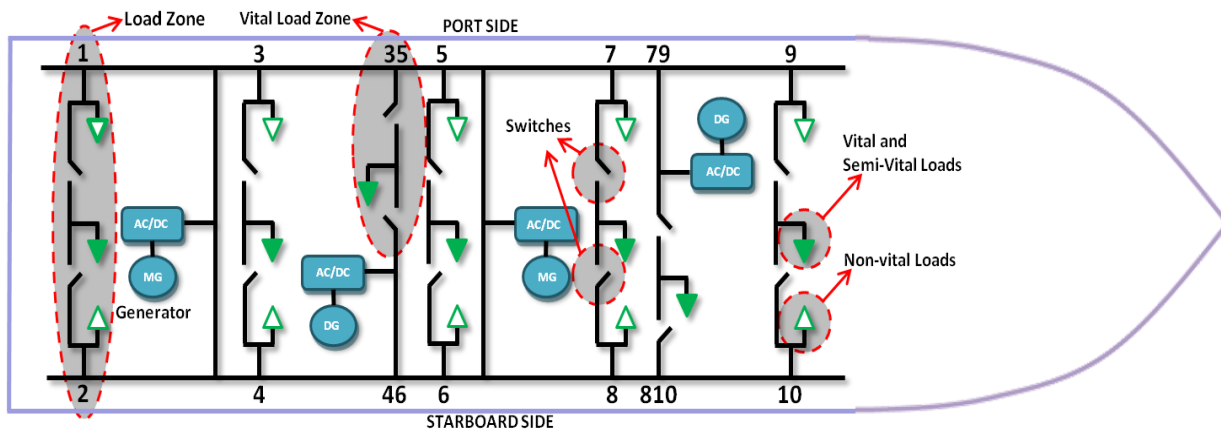


Figure 2.1 Joseph's Corzine Model of a Shipboard Power System (adapted from [1])

2.2 Energy Storage Device

Amanuel Kesete, in his thesis titled “Optimization of storage integrations into MVDC in shipboard power system” [8], a comprehensive Li-Ion battery model. This model has been directly used in this research with a few parameters changes. The detailed introduction of this model will be discussed in Chapter 4.

2.3 Real Time Simulation

2.3.1 Introduction of Real Time Simulation

Simulation tools have got a rapid evolution from the analog simulators at the beginning to the digital simulators in the past decades. At present, the digital simulators have been used widely in a number of industries. Especially, the real-time simulation, based on automatic code generation, has played vital role in many engineering field and applications, such as industrial

motor drive design, complex robotic controller design and power grid statistical protection tests [2].

2.3.2 Function of Real-time simulation

The real-time simulation can be defined as a virtual model established by computer on the basis of the objective physical system. It can work at the same rate as actual "wall clock" time, namely, the actual physical time. With this capability in nature, a real-time simulator can bring benefits to industrial design in many aspects. Generally, the functions of the real-time simulation can be divided into three categories [2]:

- Rapid control prototyping (RCP)
- Hardware-in-the-loop (HIL)
- Pure simulation (PS)

In the RCP function, a proposed controller archetype is established into a virtual model by a real-time simulator and connected with physical plant by I/O port. Instead of testing a physical controller, a virtual model provides a more flexible, faster and more economical way for controller debug [3].

The HIL simulation aims to provide an effective platform for developing and testing physical controller. Through HIL simulation, the designed controller no longer needs to wait for a physical plant to write or test code. The plant is able to be replaced by a virtual model established by a real-time simulator, in which the testing can include the simulation for large versions of the plant, such as a high power generator. Usually, it is risky to test a controller in a large physical plant. Especially, testing the physical controller in some extreme case, such as simulation of over burdening, would likely destroy a physical plant [3]. For these facts, the HIL

simulation is introduced to work as an effective platform in a controller testing, especially for the case of some very complicated plants which are hardly achieved in physical model [3].

Unlike RCP and HIL involving physical model in test, PS mode employs virtual models to take the places of both controller and plant in the real-time simulation. Since there is no input and output signals between virtual model and physical model, the signal loss existed in RCP and HIL is able to be eliminated in PS mode [4]. As a result, the test in PS mode will be more accurate than RCP and HIL mode without the influence of signal loss. Moreover, PS mode can also provide a faster simulating speed than real-time with no impact on the validity of results [4].

2.3.3 RT-LAB for Real Time Simulation

As a real-time simulation platform, the RT-LAB software is used to achieve high-fidelity plant simulation control system prototyping, and embedded data acquisition and control.[] Meanwhile, its distributed processing capability also allows users to quickly convert Simulink or System build models to high-speed, real-time simulations, over one or more target PC processors [5].

In order to realize complicated electrical systems in real-time simulation and improve accuracy of the result, the RT-LAB Electrical Drive Simulator comes with some special Simulink-based modeling tools, such as ARTEMIS and RT-Events, which permits the real-time simulation of an electrical system at practical time step of $10\mu s$.

ARTEMIS and RT-Events are mainly used in this study.

ARTEMiS toolbox

ARTEMiS works as a plug-in blockset under the SimPowerSystem and helps to improve distributed simulation of power systems over multiple processors [6]. Other than normal simulations whose objective is to minimize total simulation time or the smallest average simulation time step, a real time simulation is proposed to get a smaller maximum time step to fulfill the operating rate of the external physical devices in the simulation while keeping the accuracy in a certain extent [6]. Moreover, ARTEMiS also offers a new solver called State-Space Nodal which combines the accuracy potential of state-space methods with the natural ability of the nodal approach to handle circuit with a large number of switches.

RT-Events toolbox

Similar to ARTEMiS, RT-Events is another blockset that can be used with the Simulink software and that enables the simulation of event-based systems that comprise continuous- and discrete-time subsystems whose dynamics changes due to discrete events [6]. Generally, RTEvent is introduced to solve following problem encountered in the simulation of event-based systems. During a simulation, errors would be introduced by the situations that some switching events may occur between the sampling instances or multiple events occur in a single time step [6].

From Simulink based design to Real-Time module by RT-Lab

RT-LAB uses Simulink to define models and corresponding parameters which will be executed by the real-time multi-processing system [7]. After the model of integrated Shipboard

Power System is implemented in Matlab Simulink, several more steps have to be completed to realize the real-time model in the RT-Lab software and hardware [7].

1. Regroup into subsystems
2. Add the OpComm block(s)
3. Maximize parallel execution and state variables
4. Set the real-time parameters
5. Run offline

2.4 Conclusion

Shipboard power system and battery model have been developed for incorporation and integration. However, there is a lack of development in bidirectional DC/DC converter and energy management subsystem for this power system to be connected and controlled. In the meanwhile, SPS and ESDs need to be modulated in size and configuration to apply to this research. This thesis will look for a novel method to develop an energy management system to integrate the backup energy storage device and the shipboard power system.

Chapter 3 - Models of the Shipboard Power System

In this chapter, shipboard power system (SPS) models are presented. The first model was provided by the United States Office of Naval Research with complex system. The second model, a simplified model that realistically represents the shipboard system, was used in this study to fit the number of CPU in the Real-Time Simulator. The systems were simulated in MATLAB Simulink using the SimPowerSystems toolbox, ARTEMIS, and RT-Events plug-in blockset.

3.1 Corzine Model of the Shipboard Power System

The Corzine Model of the SPS was provided by the United States Office of Naval Research. This model has four generators in the system: two distributed generators produce 4 MW and two main generators operate at 6 MW [1]. The Corzine model has five load zones containing two non-vital loads, one semi-vital load, and one vital load. Switches connect higher priority loads to the port side or starboard bus. In addition, two load zones are added between a generator and a bus, as shown in Figure 3.1. These two new loads represent single vital load SPS motors connected to one bus and a generator through switches.

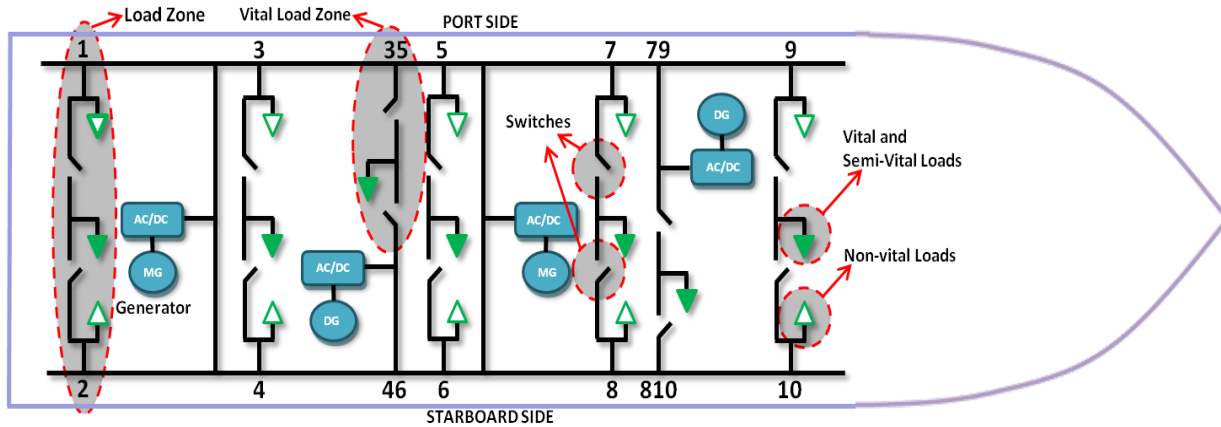


Figure 3.1 Corzine Model of a Shipboard Power System

3.2 Simplified Model of the Shipboard Power System

All-electric warships will be equipped with highly complex energy generation and distribution systems that operate well under severe conditions. Therefore, this system includes power electronics systems connected by AC and DC busses to feed a variety of complex controls and loads. The system is useful for the formation and implementation of new, knowledgeable concepts due to the complexity of the interconnected system. In particular, the stability of such systems is important.

This model carries two synchronous machine generators, shown in Figure 3.2. In the system, each generator feeds one DC bus. From each bus, a buck converter feeds each load in a redundant way so the load can be fed from the other bus if power fails. Three load zones are connected to the buses: a synchronous motor, AC loads, and a CPL.

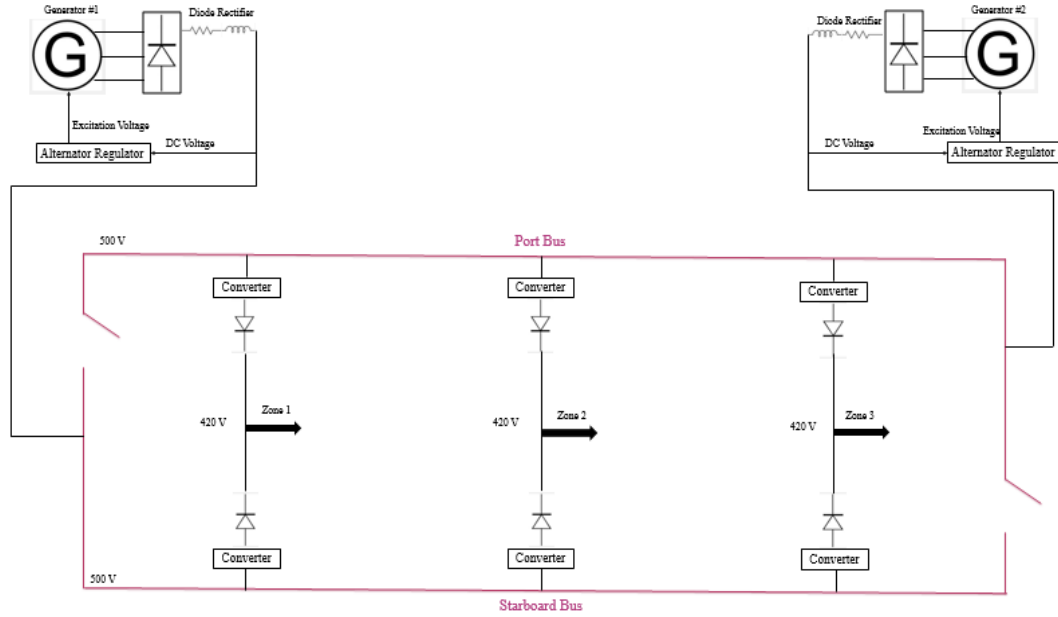


Figure 3.2 Simplified Model of Shipboard Power System

3.2.1 Simulation of Generators

The generator is a 500 Vdc, 2 pole, 30 kW Synchronized Machine with the associated drive (based on AC6 blocks of the SimPowerSystems Electric Drives library). A diesel motor and speed regulator is used to achieve a maximum motor speed of 13000 rpm. The generator and a rectifier were integrated into one subsystem in the simulation, as shown in Figure 3.3. A simplified synchronous machine model was used to simulate power produced. After the machine, a rectifier was attached to convert three-phase AC output voltage to DC voltage. Output voltage after the rectifier is the required bus voltage 500V. The measured bus voltage was compared to 500V reference voltage. The error signal goes through PI controller drives the generator to maintain the bus voltage at a 500V constant value. In order to ensure a stable bus voltage, a filter was attached to clean up noise potentially caused by the power electronics.

To place a fault in generator, the shutdown tap shown in Figure 3.4 was set to 0.

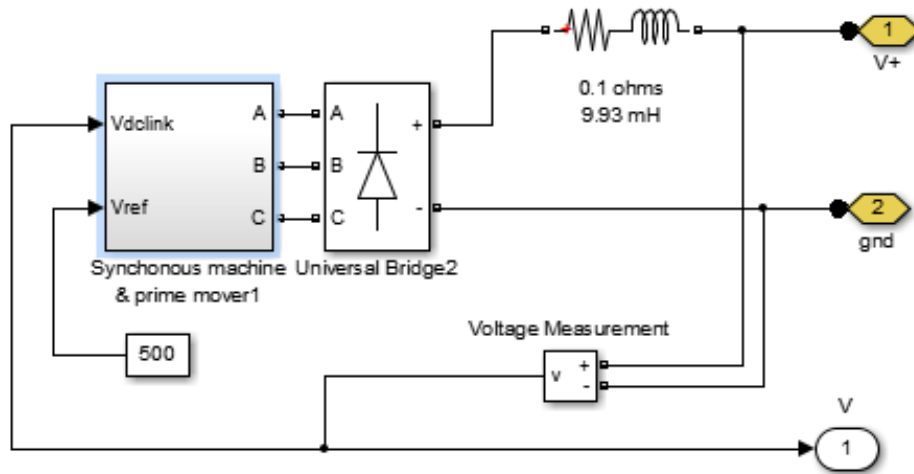


Figure 3.3 Simulation Model of Generator

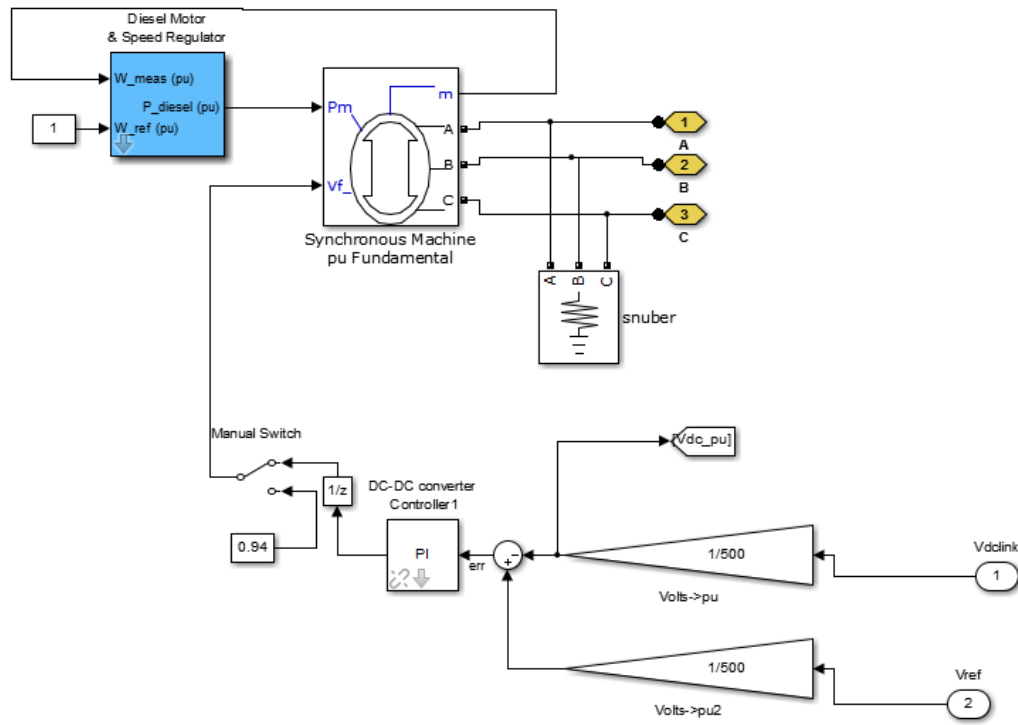


Figure 3.4 Simulation of Fault Placement on Generator

A DC-DC buck converter was then connected with the bus, as shown in Figure 3.5. A buck converter stepped down the 500 V bus voltage to 420 V to feed the loads. An additional filter was added after the buck converter to clean up noise. Output voltage of the buck converter was compared to the 420V desired voltage in order to generate an input signal for the PI controller. The PI controller control signal works on the converter switch to maintain its output value at 420V.

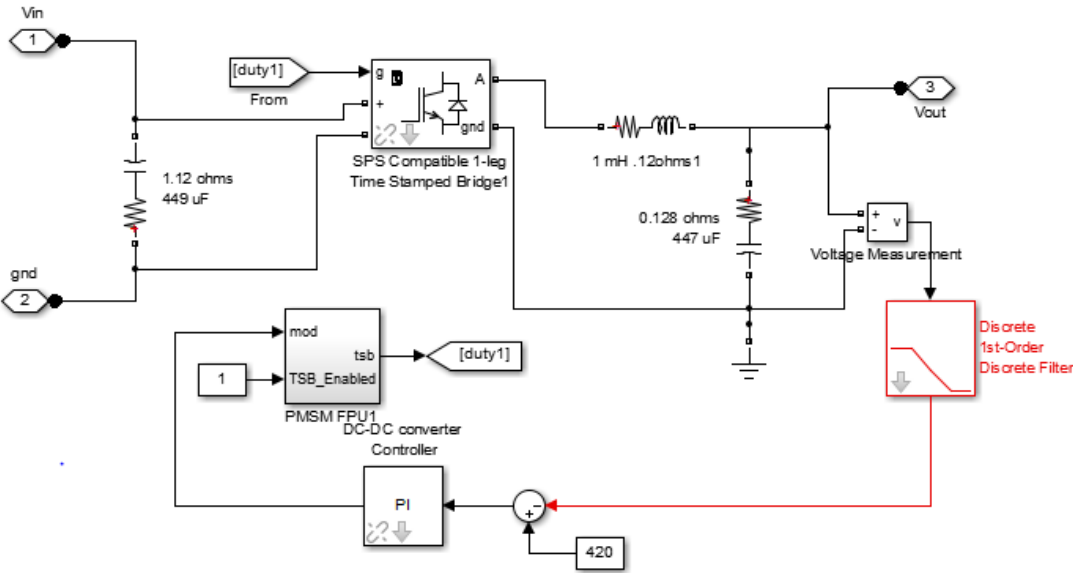


Figure 3.5 Control Diagram of the Generator Output Voltage

3.2.2 Simulation of Motor

The high-level schematic shown in Figure 3.6 is built from five main blocks. The electrical motor is a 500 Vdc, 50 kW interior Permanent Magnet Synchronous Machine (PMSM) with the associated drive (based on AC6 blocks of the SimPowerSystems Electric Drives library). This motor has 8 pole and the magnets are buried (salient rotor's type). A flux weakening vector control is used to achieve a maximum motor speed of 6 000 rpm.

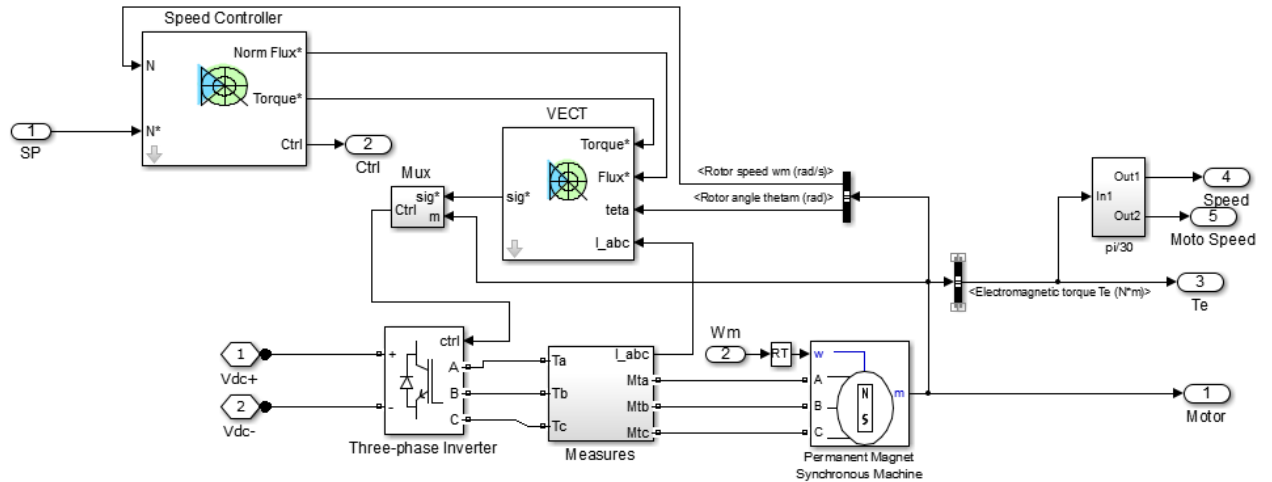


Figure 3.6 Simulation of Motor

The speed controller is based on a PI regulator with output that is a torque set point applied to a Direct Torque and Flux Control (DTC) controller block. The DTC controller uses a Torque & Flux calculator to estimate electromagnetic torque. Two look-up tables can select a specific voltage vector in accordance with the output of the Torque & Flux calculator. Consequently, the DTC controller generates switching signals for the three-phase inverter.

3.2.3 Simulation of AC Loads

Two AC loads and a 208V inverter were integrated into one subsystem in the simulation, as shown in Figure 3.7. A DC/AC inverter was connected to the DC bus to invert DC voltage to AC voltage. A filter was attached to clean up noise caused by loads down the line. A transformer was then added to step down the voltage to the required voltage of 208Vrms. A 10kW, 208 Vrms load was simulated as vital load and connected through a switch with a 10kW,

208 Vrms semi-vital load. When an outage occurs in the SPS, the switch opens to continue feeding the vital load.

Output voltage of the load was compared to the 208V reference load voltage (1 pu in this case). The error signal goes through a PI controller to generate a PWM control signal for IGBTs in the DC/AC inverter.

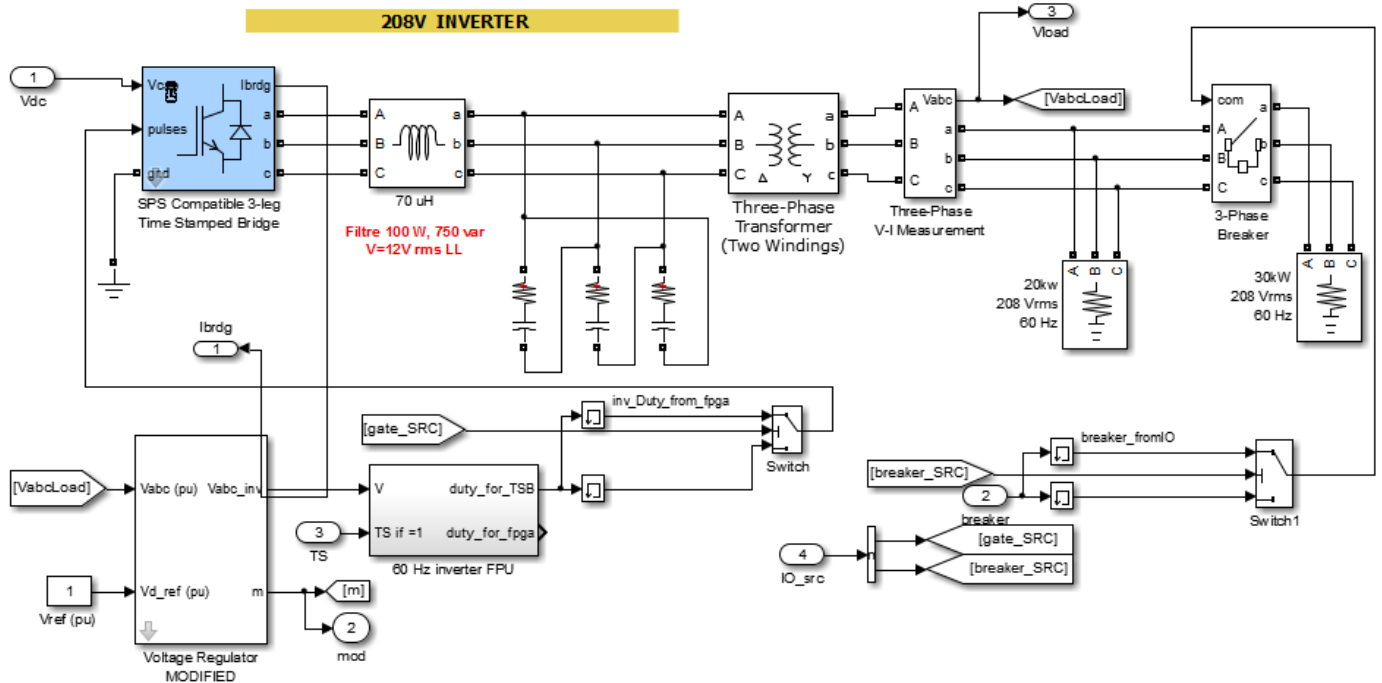


Figure 3.7 Simulation of AC Loads

3.2.4 Simulation of Constant Power Load

AC constant power load was built using the block from RT-Lab toolbox directly. A 10kW constant power load was utilized in this study.

Chapter 4 - Modes of Energy Storage Devices

Electric storage systems are crucial in order to improve quality of service of future electric ships. Reliable electric power is critical for ship operation during normal conditions and ship survivability during hostile conditions [8]. This chapter shows the development of battery and ultra-capacitor storage system models for integration with the SPS. Battery energy system, which has high energy density, is used as a backup power source in case of a power outage in the SPS [8]. Ultra-capacitor storage system is more suitable for handling short time transients or spikes because it has high power density and fast discharging rate [9].

4.1 Battery Equivalent Circuit and Simulink Model

Batteries are the most commonly used storage devices. Recent advancements in the type of material used in batteries have increased suitability of batteries for a wide range of applications [9]. Several equivalent electrical circuit models can accurately predict electrochemical battery behavior, but those models require extensive amounts of time and memory during simulation [9]. The Li-Ion battery model developed by Amanuel Kesete [8] was being used in this research. Amanuel Kesete built the battery model with capacity of 3.7 V and 2200mAh [8]. This model has the output of state of charge (SOC), terminal voltage, battery power, output current and power losses [8]. For this research, a simplified battery model was developed based on Amanuel Kesete's model which provided a good prediction of electrochemical battery behavior. The proposed Li-Ion battery model was built to predict only state of charge (SOC), terminal voltage, and battery power. 78 simplified Li-Ion battery packs model with 60 paralleled single batteries were simulated in series, giving a 13.9 Ah, 288 Vdc, 25 kW Lithium-Ion battery. This new 25 kW Li-Ion battery model was used in this research to power the shipboard power system.

4.1.1 Electrical Model and Mathematical Equations

A model must simulate the Li-Ion battery with accurate prediction of important parameters. The electrical model must accurately represent terminal voltage, SOC, and battery power without excessive simulation times. Accurate determination of discharge capacity, which is a function of the discharge rate $i(t)$, cycle number $f_3[n_{cycle}]$, and temperature $f_2[T(t)]$, must also include a rate factor $f_1[i(t)]$ [8]. The model used in this research, shown in Figure 4.1, is capable of accurately predicting SOC, terminal voltage, and power of Li-Ion battery. The equations representing SOC and $V_{terminal}$ were presented in reference [8] and were shown below:

$$SOC[i(t), T(t), n_{cycle}, t] = SOC_{initial} + \int_0^t f_1[i(t)] \times f_2[T(t)] \times f_3[n_{cycle}] \times i(t) dt$$

$$V_{terminal} = V_{oc}(SOC, T) - i_{bat}(t) \times R_{int}(SOC, T) + i_{bat}(t) \times R_{transient}(\tau_s, \tau_m, \tau_h)$$

$$R_{transient} = (R_s(SOC) e^{-\frac{1}{R_s(SOC)C_s(SOC)}t} + R_m(SOC) e^{-\frac{1}{R_m(SOC)C_m(SOC)}t} + R_h(SOC) e^{-\frac{1}{R_h(SOC)C_h(SOC)}t})$$

Equation (a) is normalized to battery capacity, so V_{SOC} lies between 0 and 100% and represents SOC of the battery [8]. $I_{battery}$ is the battery load modeled as a current source, while $R_{self-discharge}$ and R_{cap_fade} are paralleled to $C_{capacity}$, representing normalized self-discharge and battery capacity correction factors [8]. $V_{terminal}$, shown in the right circuit of Figure 4.1, relates to a multiple time-constant approach (τ_{sec} , τ_{min} , and τ_{hour}) for modeling

transient behavior of terminal voltage in which each parameter is a function of SOC [8]. This battery model has been implemented into Simulink.

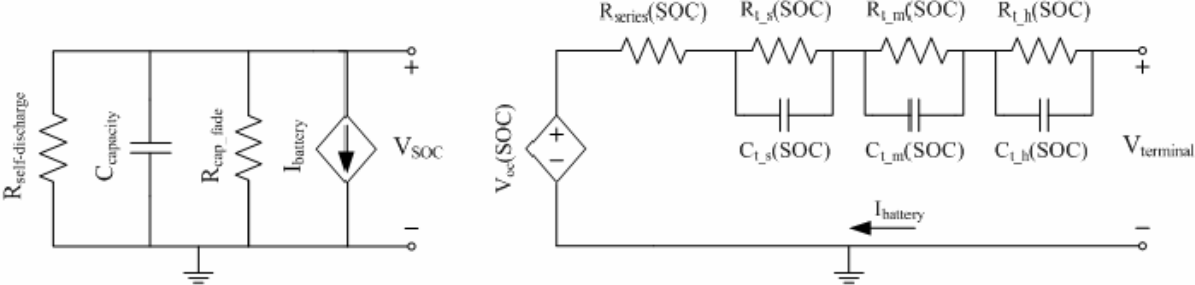


Figure 4.1 Electrical Battery Model [8]

4.1.2 Simulink Model of the Battery

For this research the model was implemented in Simulink. The Simulink model, shown in Figure 4.2, represents the storage system for SPS and contains the model shown in Figure (1). The Simulink model has three basic blocks: SOC estimation block, component and terminal voltage estimation block, and measurement block.

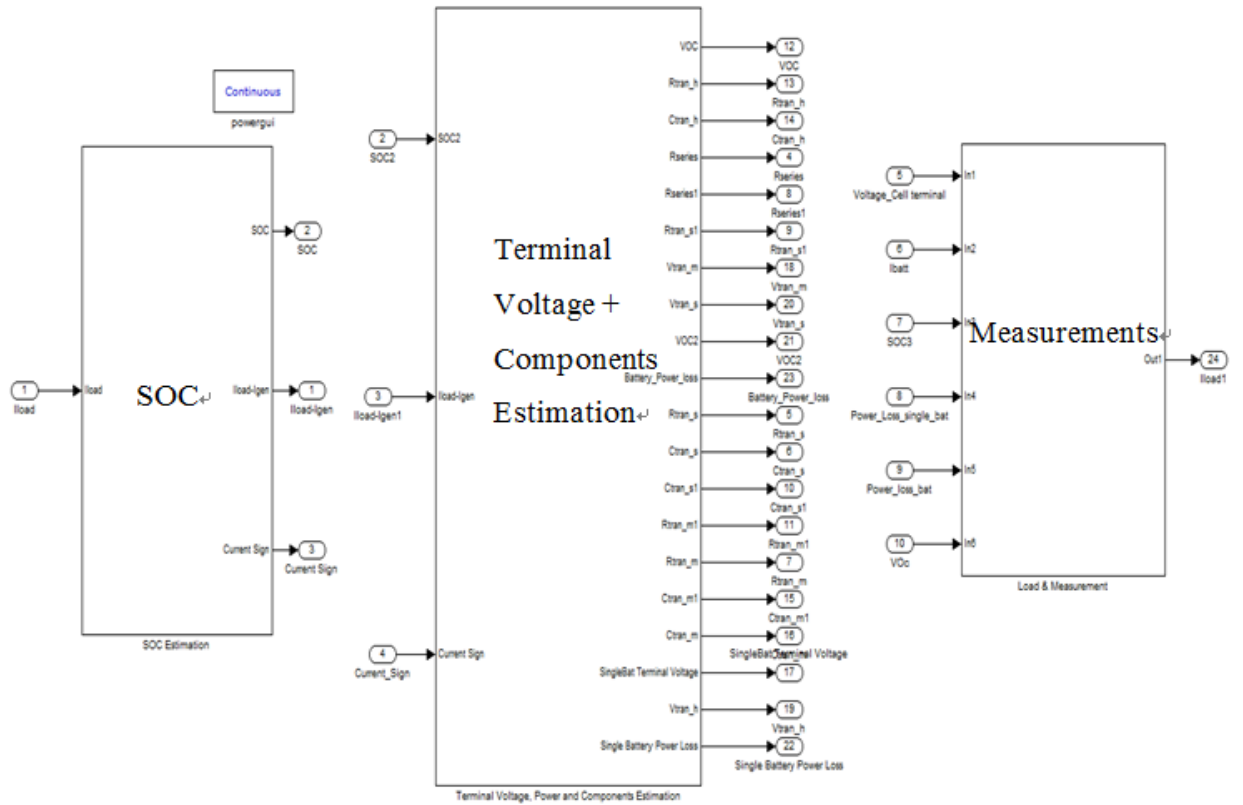


Figure 4.2 Electrical Battery Model in Simulink

The SOC estimation block in Figure 4.3 was developed based on mathematical equation (a) which calculates SOC by using I_{load} . The input signal I_{load} flows from the load to the battery during charging or from the battery to the load during discharging.

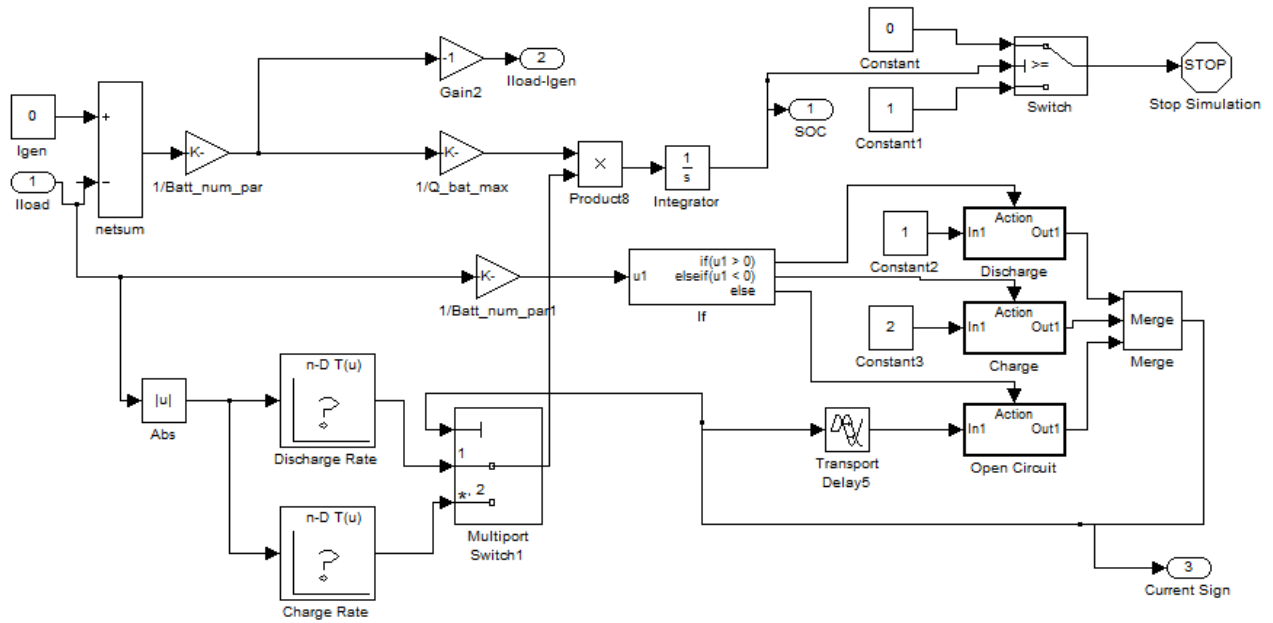


Figure 4.3 SOC Estimation Block[8]

The primary function of the SOC estimation block is to predict SOC of the battery at any time during the charging or discharging process. The block also determines the sign of the current, which indicates the mode of charging or discharging. Simulation of the model stops if SOC of the battery is below the standard SOC level (20% of the maximum SOC).

The outputs of the SOC estimation block are fed to the component and terminal voltage estimation block, as shown in Figure 4.4. This block estimates all component values of the electrical model (all resistors and capacitor values) and $V_{terminal}$. Terminal voltage of a battery is calculated using circuit parameters and current sign for SOC block and circuit parameter subsystems. Equation (b) was used to calculate battery terminal voltage. This block also estimates power output of a single cell and battery back, or power losses inside the battery. The series and parallel multipliers to the storage system then recreate a complete battery pack.

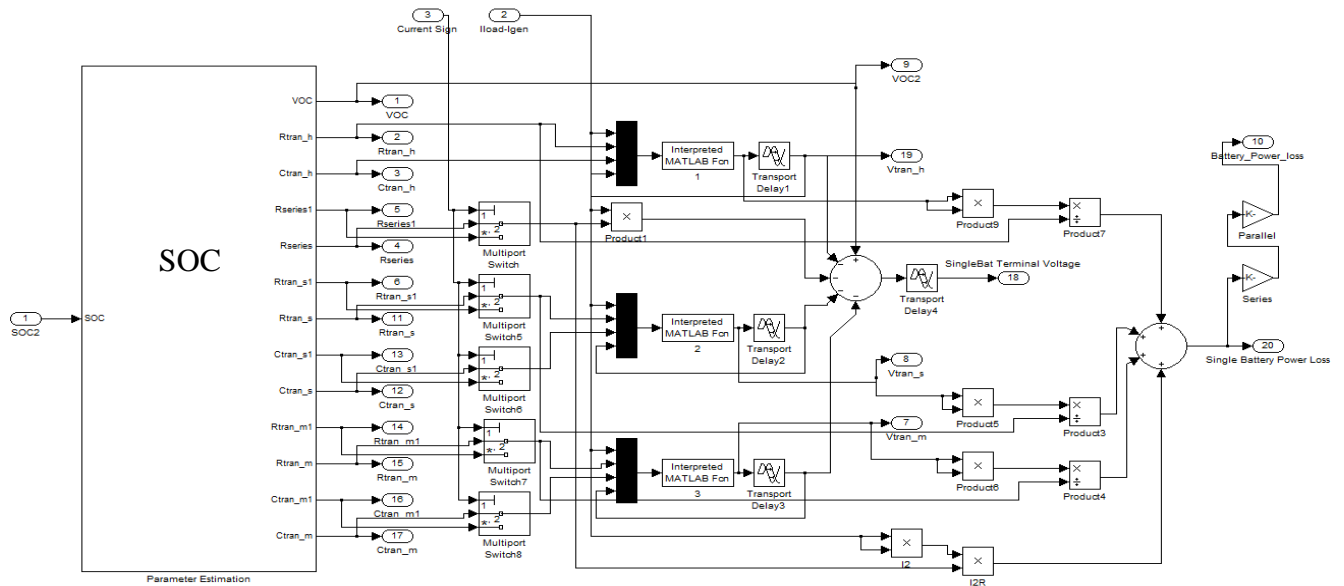


Figure 4.4 Component and Terminal Voltage Estimation Block

4.2 Ultracapacitor Equivalent Circuit and Simulink Model

Ultracapacitors are also commonly used as backup power sources capable of quickly recharging and supplying power. Compared to batteries, ultracapacitors have very high power densities and almost indefinite charging/discharging capability, making them suitable for SPS applications for handling transients [9]. Similar to Li-ion batteries, the capital cost of ultracapacitors is high, thereby generating concern regarding large-scale use [8]. The ultracapacitor modeling is explained in the following sections of this chapter.

4.2.1 Electrical Model and Mathematical Equations for Ultracapacitor

A variety of circuit models have been used in previous studies. Application requirements dictate selection of model complexity. The equivalent circuit of the ultracapacitor is shown in Figure 4.5 [10]. The model that has been selected represents only the electrical properties of the cell and neglects most of the chemical properties [10].

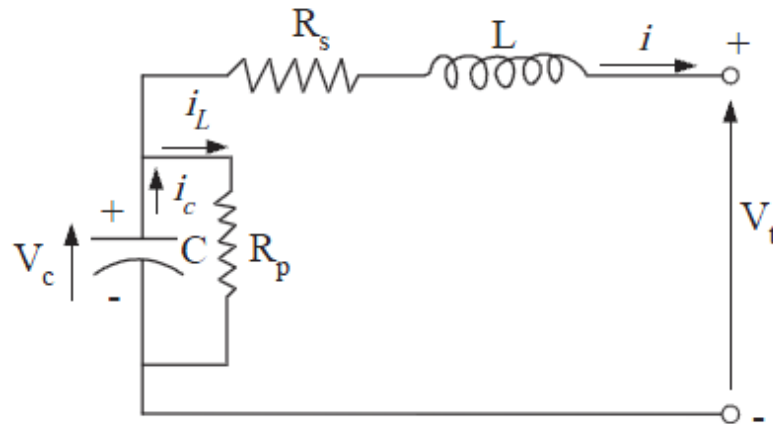


Figure 4.5 Simplified Electric Model for Ultracapacitor [8]

Based on the model in Figure 4.5, the equations of the circuit were developed and used to model the ultracapacitor [10]. The primary voltage and current equations used were:

$$V_t = V_c - R_s i + L \frac{di}{dt}$$

$$V_c = V_c^0 - C \int_0^t i_c dt$$

$$i_L = \frac{V_c}{R_p}$$

$$i_c = i + i_L$$

The mathematical model based on the equations is shown in Figure 4.6.

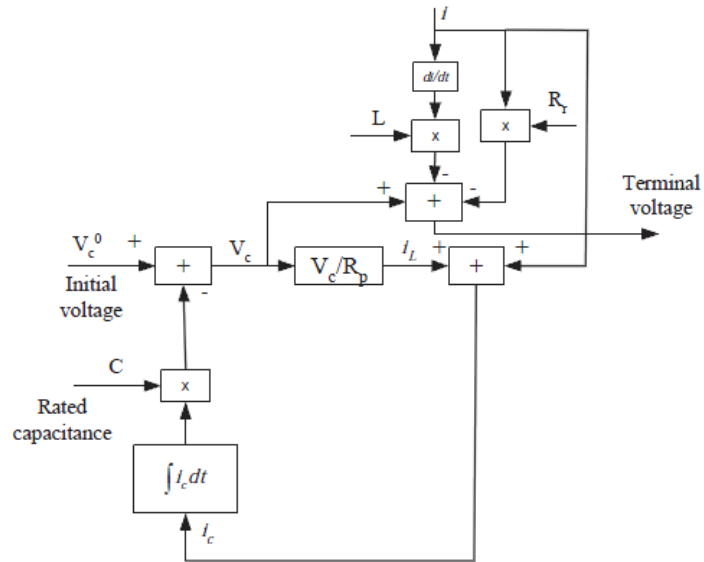


Figure 4.6 Mathematical Model for Ultracapacitor[8]

4.2.2 Simulink Model of the Ultracapacitor

Based on the electric model and mathematical model presented in previous sections, a model of the ultracapacitor was built in Simulink, as shown in Figure 4.7. The voltage level of the ultracapacitor can increase or decrease by changing the resistance values, capacitance, and number of cells in series and in parallel [11].

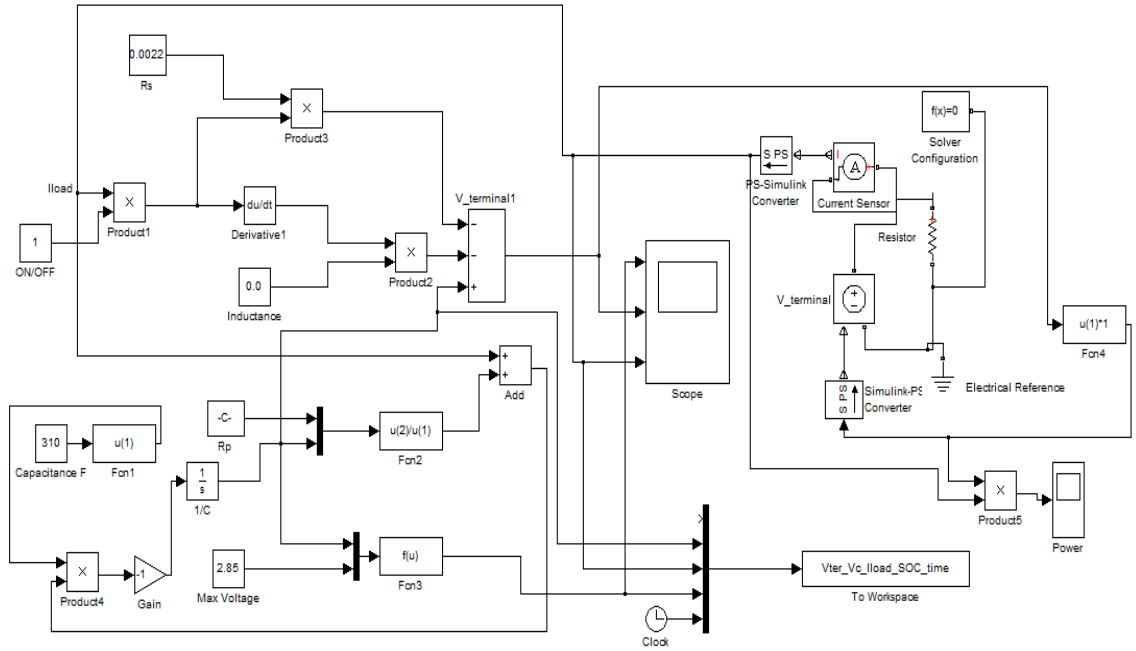


Figure 4.7 Simulink Model for Ultracapacitor [11]

4.3 Summary

This chapter provides an overview of the mathematical models and simulink models for Li-Ion battery and ultracapacitors. Performance of the battery pack combined with SPS are presented in Chapter 7.

Chapter 5 - Model of the Bi-directional DC-DC Converter

Currently, bi-directional DC-DC converters are widely researched and developed for various applications, such as battery charger-dischargers, hybrid power systems, and SPS [12]. For this thesis, electric energy flows between the battery and generator side and the battery and motor side. The use of a bi-directional DC-DC converter allows stable control for motoring and regenerative braking operations for SPS application and significantly increases overall efficiency of the drive system. A closed loop control technique was designed and implemented using PI controller.

A detailed mathematical analysis of the bi-directional DC-DC converter under steady state and transient condition is presented. Mathematical models for buck and boost modes were derived and the Matlab Simulink model was constructed to be used for this research and was integrated with the SPS.

5.1 Bi-directional DC-DC Converter Control Strategy

The proposed bi-directional DC-DC converter is shown in Figure 5.1. Buck mode and boost mode were built to have opposite inductor current directions [13]. In this topology, boost converter operation is achieved by modulating $Q2$ with the anti-parallel diode $D1$ serving as the boost-mode diode. In addition, the topology functions as a buck converter through the modulation of $Q1$, with the anti-parallel diode $D2$ serving as the buck-mode diode [13]. A control model was developed using PI controller to achieve charging and discharging of the battery [13]. Two simplified battery models designed in Chapter 4 were used to verify converter performance.

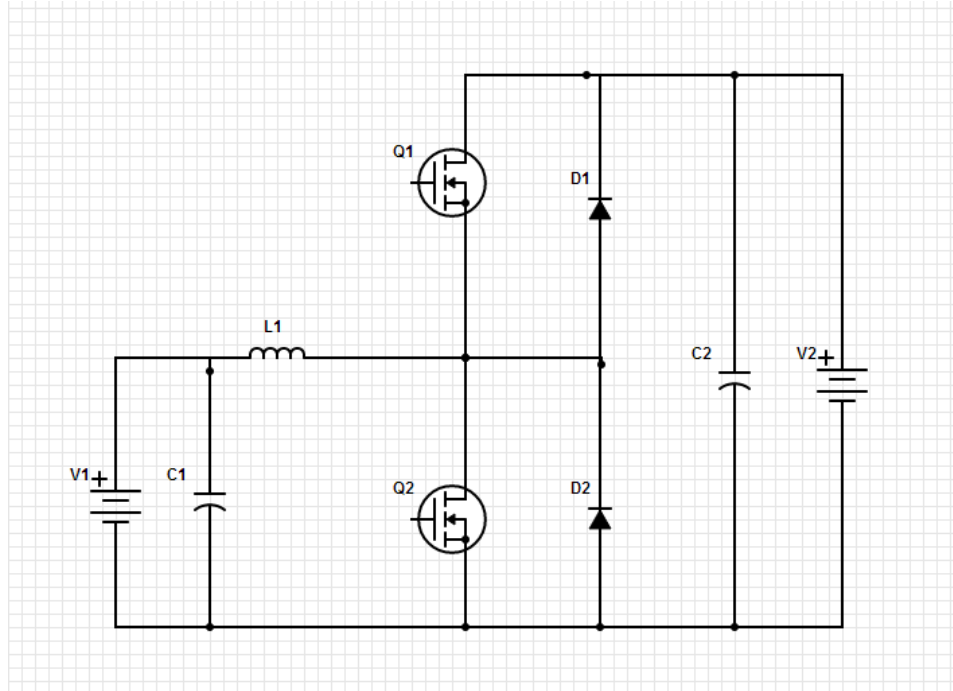


Figure 5.1 Power Circuit of a Bidirectional DC-DC Converter

The control circuit of the bi-directional converter is shown in Figure 5.2. In order to guarantee that the battery model is charged when its SOC is lower than standard level, the output voltage of the bi-directional converter was controlled by a PI controller. In this control technique, the output voltage of the converter v was measured and compared with a reference battery voltage v_{ref} .

The error signal between measured voltage and reference voltage was processed through the PI controller. The error signal was then compared to a saw tooth signal with switching frequency to generate control signals for pulse width modulated (PWM) [14]. The control circuit is shown in Figure 5.2.

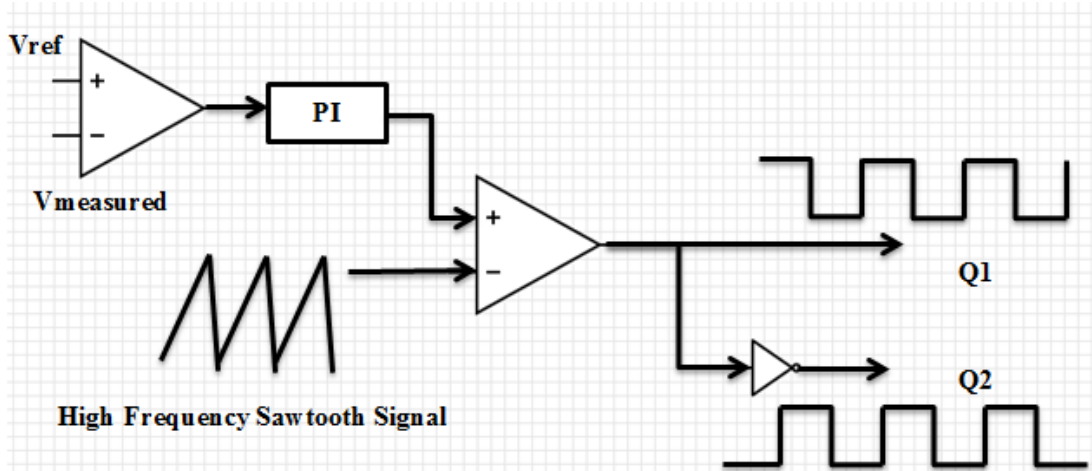


Figure 5.2 Control Circuit for Bidirectional DC-DC Converter

5.2 Bi-directional DC-DC Converter Matlab Simulink Model

Once the power circuit for bi-directional DC-DC converter was designed, the circuit was analyzed, and the Simulink model was built and verified

5.2.1 Dynamic Analysis of the Bi-directional DC-DC Converter

Typical configuration of a power circuit for a bi-directional DC-DC converter with voltage and current parameters is shown in Figure 5.3. When the DC-DC converter operates as a boost or buck converter in continuous conduction mode, current in the inductor flows continuously [15]. Dotted arrows indicate current direction in a buck mode, while black arrows indicate current

direction in a boost operation. Based on this power circuit, the output and input voltages and inductor current can be derived.

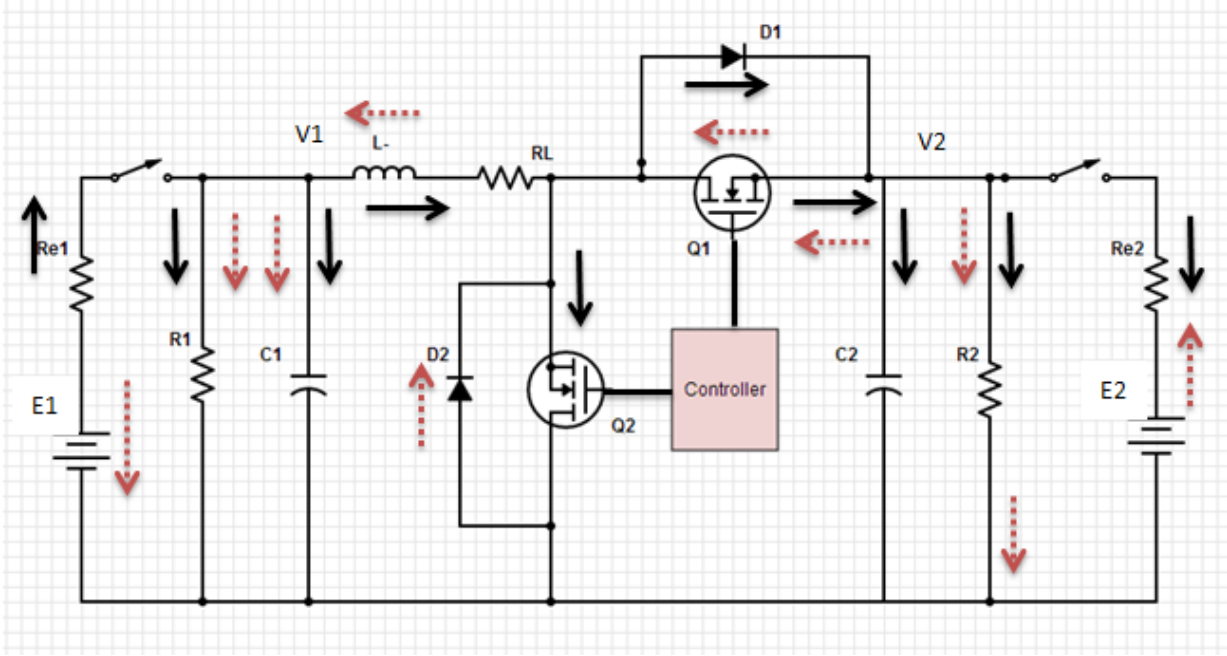


Figure 5.3 Voltages and Currents for Boost and Buck DC-DC Converter

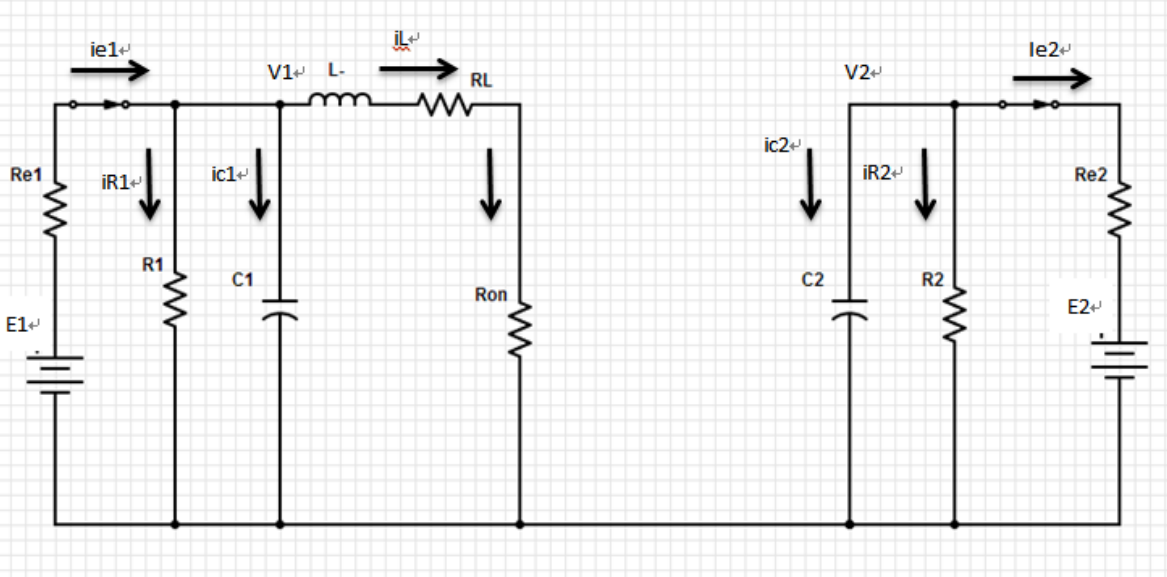


Figure 5.4 Interval 1: Voltages and Currents for Boost DC-DC Converter

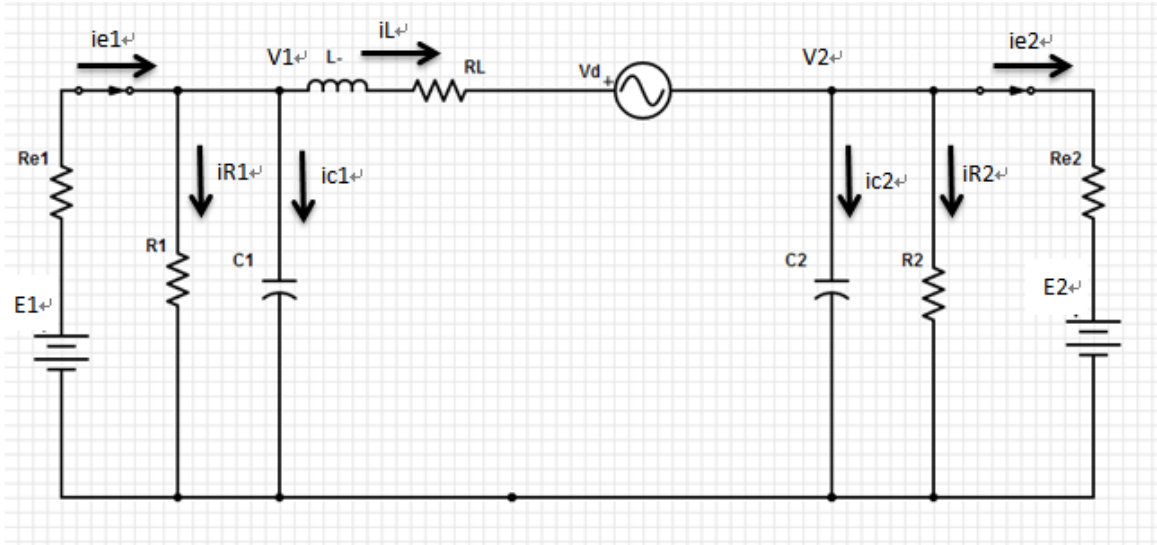


Figure 5.5 Interval 2: Voltages and Currents for Boost DC-DC Converter

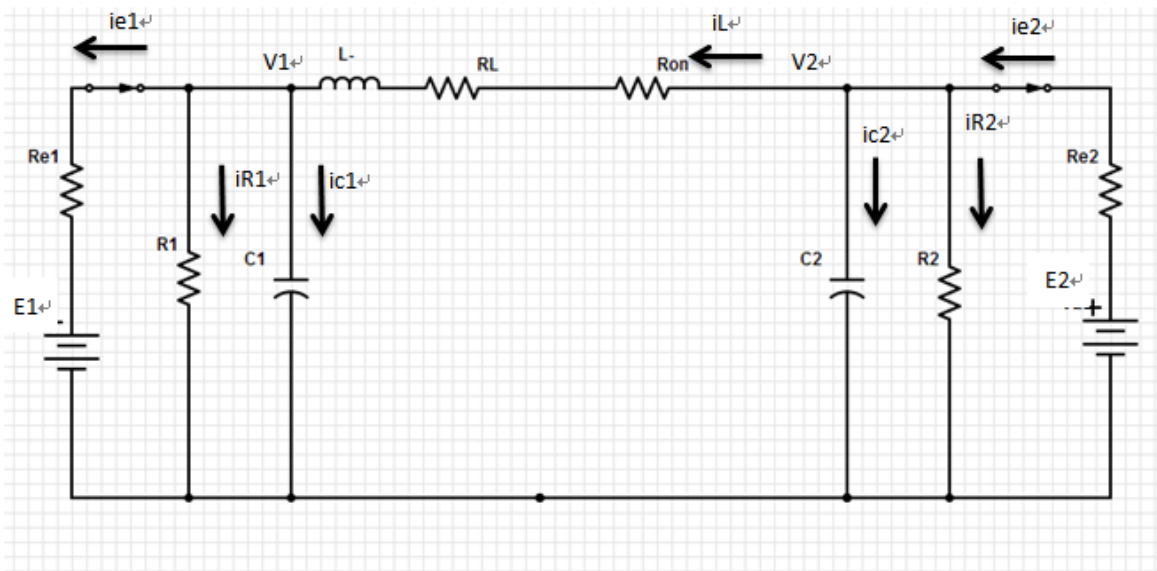


Figure 5.6 Interval 1: Voltages and Currents for Buck DC-DC Converter

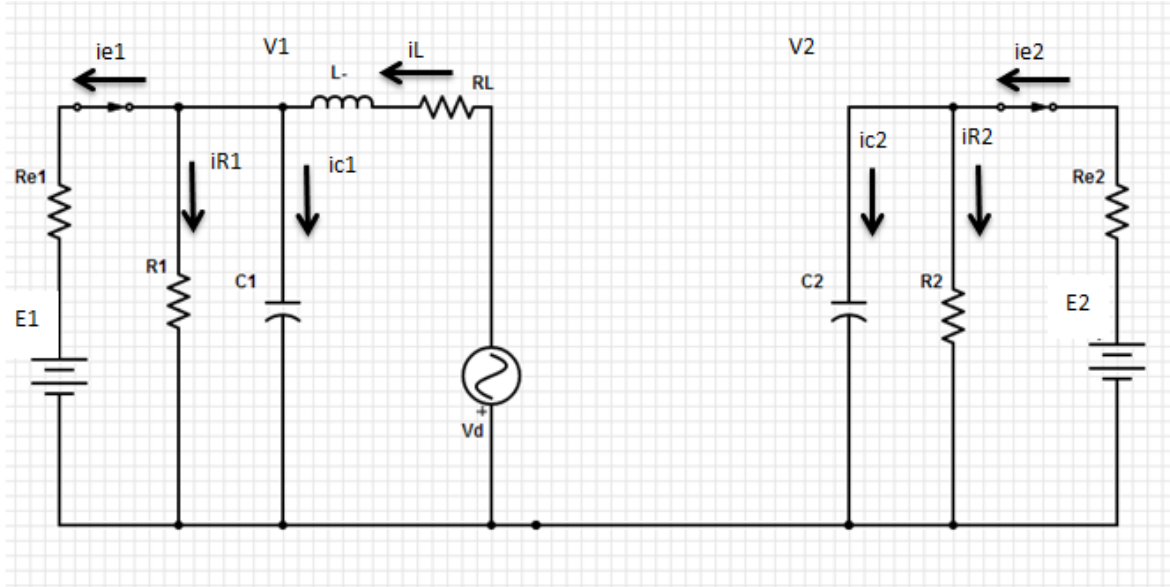


Figure 5.7 Interval 2: Voltages and Currents for Buck DC-DC Converter

Boost Mode:

Interval 1: At time t_0 , the lower switch Q_2 is turned ON and the upper switch Q_1 is turned OFF with diode D_1 , D_2 reverse biased, as shown in Figure 5.4. During this time interval, the converter operates in boost mode, the inductor is charged, and current increases through the inductor. Application of Kirchhoff's voltage law to the loop gives:

$$i_{e1} = \frac{E_1 - V_1}{R_{e1}}; \quad i_{R1} = \frac{V_1}{R_1}; \quad i_{c1} = C_1 * \frac{dV_1}{dt};$$

$$i_{c1} = i_{e1} - i_{R1} - i$$

$$\frac{dV_1}{dt} = \frac{1}{C_1} * i_{c1} = \frac{1}{C_1} \left(\frac{E_1 - V_1}{R_{e1}} - \frac{V_1}{R_1} - C_1 * \frac{dV_1}{dt} \right) \dots\dots$$

$$V_L = L \frac{di}{dt} = V_1 - (R_L + R_{on})i$$

$$\frac{di}{dt} = (V_1 - (R_L + R_{on})i)/L \dots$$

And

$$i_{e2} = \frac{-E_2 + V_2}{R_{e2}}; \quad i_{R2} = \frac{V_2}{R_2}; \quad i_{c2} = C_2 * \frac{dV_2}{dt};$$

$$\frac{dV_2}{dt} = \frac{1}{C_2} * i_{c2} = \frac{1}{C_2} (-i_{R2} - i_{e2}) = \frac{1}{C_2} \left(-\frac{V_2}{R_2} - \frac{-E_2 + V_2}{R_{e2}} \right)$$

Interval 2: When MOSFET $Q2$ is switched off at $t = t1$, the inductor is connected between the input and output voltages through diode $D1$ and the current that is flowing through MOSFET $Q2$ will now flow through L , $D1$, $C2$, and load $R2$, as shown in Figure 5.5. Application of Kirchhoff's voltage law to the loop gives:

$$i_{e1} = \frac{E_1 - V_1}{R_{e1}}; \quad i_{R1} = \frac{V_1}{R_1}; \quad i_{c1} = C_1 * \frac{dV_1}{dt};$$

$$i_{c1} = i_{e1} - i_{R1} + i$$

$$\frac{dV_1}{dt} = \frac{1}{C_1} * i_{c1} = \frac{1}{C_1} \left(\frac{E_1 - V_1}{R_{e1}} - \frac{V_1}{R_1} + i \right) \dots$$

For V_L :

$$V_L = -V_1 - R_L i - V_D; \quad \frac{di}{dt} = V_1/L$$

$$\frac{di}{dt} = (V_1 - R_L i - V_D)/L \dots$$

For i_c :

$$i_{e2} = \frac{E_2 - V_2}{R_{e2}}; \quad i_{R2} = \frac{V_2}{R_2}; \quad i_{c2} = -C_2 * \frac{dV_2}{dt};$$

$$i_{c2} = i_{R2} - i_{e2}$$

$$\frac{dV_2}{dt} = \frac{1}{C_2} \left(\frac{V_2}{R_2} - \frac{E_2 - V_2}{R_{e2}} \right)$$

In matrix form, the equations can be represented

$$x = \begin{bmatrix} V_1 \\ i \\ V_2 \end{bmatrix}, \quad v = \begin{bmatrix} E_1 \\ V_D \\ E_2 \end{bmatrix}$$

Then,

$$\dot{x} = (DA_1 + (1 - D)A_2)x + (DB_1 + (1 - D)B_2)v$$

At steady state,

$$\dot{x} = 0$$

$$x = -(DA_1 + (1 - D)A_2)^{-1} * (DB_1 + (1 - D)B_2)v$$

$$A1 = \begin{bmatrix} -\left(\frac{1}{R_{e1} C_1} + \frac{1}{R_1 C_1}\right) & -\frac{1}{C_1} & 0 \\ \frac{1}{L} & -\frac{R_L + R_{on}}{L} & 0 \\ 0 & 0 & -\left(\frac{1}{R_{e2} C_2} + \frac{1}{R_2 C_2}\right) \end{bmatrix}$$

$$B1 = \begin{bmatrix} \frac{1}{R_{e1} C_1} & 0 & 0 \\ 0 & 0 & 0 \\ 0 & 0 & \frac{1}{R_{e2} C_2} \end{bmatrix}$$

$$A2 = \begin{bmatrix} -\left(\frac{1}{R_{e1} C_1} + \frac{1}{R_1 C_1}\right) & \frac{1}{C_1} & 0 \\ -\frac{1}{L} & -\frac{R_L}{L} & 0 \\ 0 & \frac{1}{C_2} & -\left(\frac{1}{R_{e2} C_2} + \frac{1}{R_2 C_2}\right) \end{bmatrix}$$

$$B2 = \begin{bmatrix} \frac{1}{R_{e1} C_1} & 0 & 0 \\ 0 & \frac{1}{L} & 0 \\ 0 & 0 & \frac{1}{R_{e2} C_2} \end{bmatrix}$$

Buck Mode:

Interval 1: When stepping down, MOSFET $Q1$ is on and MOSFET $Q2$ is off, and inductor current flows directly to the output, as shown in Figure 5.6. Application of Kirchhoff's voltage law to the loop gives:

$$i_{e1} = \frac{-E_1 + V_1}{R_{e1}}; \quad i_{R1} = \frac{V_1}{R_1}; \quad i_{c1} = C_1 * \frac{dV_1}{dt};$$

$$i_{c1} = -i_{e1} - i_{R1} + i$$

$$\frac{dV_1}{dt} = \frac{1}{C_1} * i_{c1} = \frac{1}{C_1} \left(\frac{E_1 - V_1}{R_{e1}} - \frac{V_1}{R_1} + i \right)$$

$$V_L = L \frac{di}{dt} = V_2 - (R_L + R_{on})i - V_1$$

$$\frac{di}{dt} = (V_2 - (R_L + R_{on})i - V_1) / L$$

And

$$i_{e2} = \frac{E_2 - V_2}{R_{e2}}; \quad i_{R2} = \frac{V_2}{R_2}; \quad i_{c2} = C_2 * \frac{dV_2}{dt};$$

$$\frac{dV_2}{dt} = \frac{1}{C_2} * i_{c2} = \frac{1}{C_2} (-i_{R2} + i_{e2} - i) = \frac{1}{C_2} \left(-\frac{V_2}{R_2} + \frac{E_2 - V_2}{R_{e2}} - i \right)$$

Interval 2: When MOSFET $Q1$ is switched off at $t = t1$, current in the inductor flowing through

MOSFET $Q1$ will now flow through diode $D2$, as shown in Figure 5.7. Application of

Kirchnoff's voltage law to the loop gives:

$$i_{e1} = \frac{-E_1 + V_1}{R_{e1}}; \quad i_{R1} = \frac{V_1}{R_1}; \quad i_{c1} = C_1 * \frac{dV_1}{dt};$$

$$i_{c1} = -i_{e1} - i_{R1} + i$$

$$\frac{dV_1}{dt} = \frac{1}{C_1} * i_{c1} = \frac{1}{C_1} \left(\frac{E_1 - V_1}{R_{e1}} - \frac{V_1}{R_1} + i \right)$$

For V_L :

$$V_L = -V_1 - R_L i - V_D; \quad \frac{di}{dt} = V_1/L$$

$$\frac{di}{dt} = (V_1 - R_L i - V_D)/L$$

$$i_{e2} = \frac{E_2 - V_2}{R_{e2}}; \quad i_{R2} = \frac{V_2}{R_2}; \quad i_{c2} = -C_2 * \frac{dV_2}{dt};$$

$$i_{c2} = -i_{R2} + i_{e2}$$

$$\frac{dV_2}{dt} = \frac{1}{C_2} \left(\frac{V_2}{R_2} - \frac{E_2 - V_2}{R_{e2}} \right)$$

In matrix form, the equations can be represented as:

$$x = \begin{bmatrix} V_1 \\ i \\ V_2 \end{bmatrix}, \quad v = \begin{bmatrix} E_1 \\ V_D \\ E_2 \end{bmatrix}$$

Then,

$$\dot{x} = (DA_1 + (1 - D)A_2)x + (DB_1 + (1 - D)B_2)v$$

At steady state,

$$\dot{x} = 0$$

$$x = -(DA_1 + (1 - D)A_2)^{-1} * (DB_1 + (1 - D)B_2)v$$

$$A1 = \begin{bmatrix} -\left(\frac{1}{R_{e1} C_1} + \frac{1}{R_1 C_1}\right) & -\frac{1}{C_1} & 0 \\ \frac{1}{L} & -\frac{R_L + R_{on}}{L} & 0 \\ 0 & 0 & -\left(\frac{1}{R_{e2} C_2} + \frac{1}{R_2 C_2}\right) \end{bmatrix}$$

$$B1 = \begin{bmatrix} \frac{1}{R_{e1} C_1} & 0 & 0 \\ 0 & 0 & 0 \\ 0 & 0 & \frac{1}{R_{e2} C_2} \end{bmatrix}$$

$$A2 = \begin{bmatrix} -\left(\frac{1}{R_{e1} C_1} + \frac{1}{R_1 C_1}\right) & \frac{1}{C_1} & 0 \\ -\frac{1}{L} & -\frac{R_L}{L} & 0 \\ 0 & \frac{1}{C_2} & -\left(\frac{1}{R_{e2} C_2} + \frac{1}{R_2 C_2}\right) \end{bmatrix}$$

$$B2 = \begin{bmatrix} \frac{1}{R_{e1} C_1} & 0 & 0 \\ 0 & \frac{1}{L} & 0 \\ 0 & 0 & \frac{1}{R_{e2} C_2} \end{bmatrix}$$

5.2.2 Simulink Models of the Converter

Based on the design of the power and control circuits presented in Section 5.2.1, an equivalent Matlab Simulink model of the bi-directional DC-DC converter was constructed, as shown in Figure 5.8. A PI controller was used to implement the system control design in order to generate a PWM signal to drive the switches in this Simulink model.

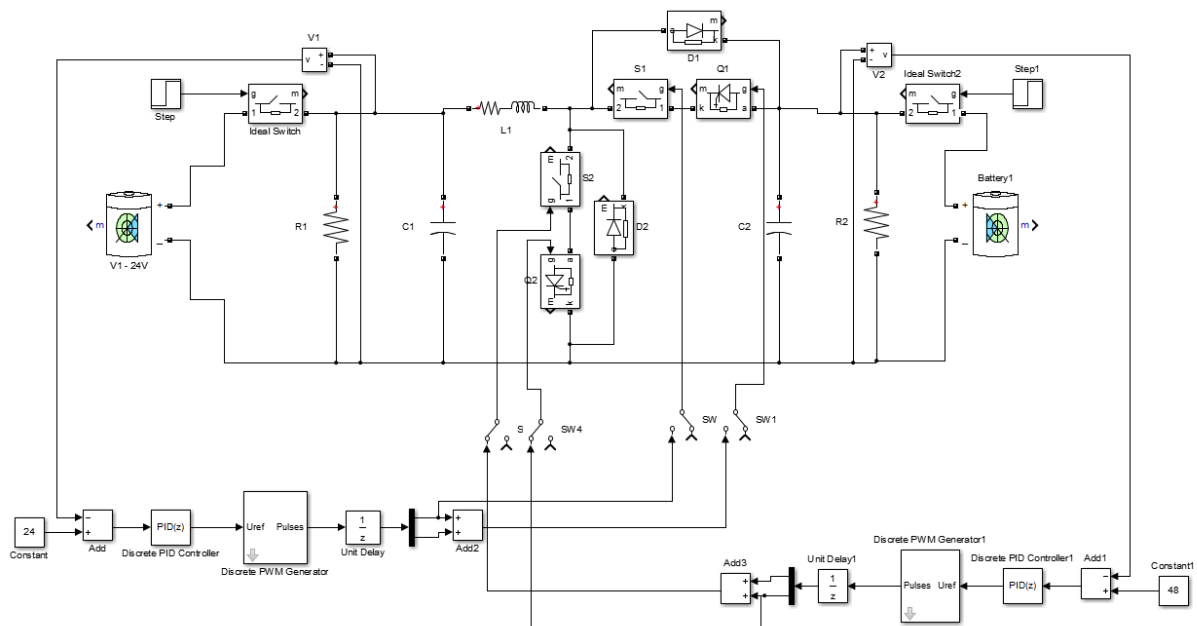


Figure 5.8 Simulink model of the bi-directional DC-DC converter

5.3 Matlab Simulink Results of the Bi-directional DC-DC Converter

Test results of this model is attached in the appendix. Converter performance using SPS application is presented in Chapter 7.

Chapter 6 - Energy Management System

The Energy Management Subsystem (EMS) represents a vital part in this simulation because it determines required torque of the electrical motor and required torque of the generator, according to maximum battery power and battery SOC. Required SPS power depends on the acceleration speed changes curve which varies between -100% (full brake) and +100 % (full acceleration). There are two subsystems in the EMS: the Battery Management Subsystem and the Power Management Subsystem.

6.1 Battery Management Subsystem

The battery management subsystem, shown in Figure 6.1, maintains the State-Of-Charge (SOC) between 40 and 80%. Also, it prevents voltage collapse by controlling the power required from the battery.

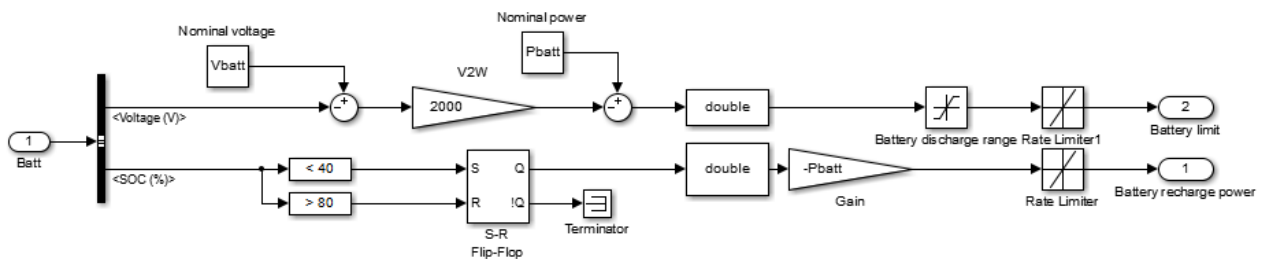


Figure 6.1 Battery Management Subsystem

The output voltage and SOC from battery model becomes the input signal of this battery management subsystem. The SOC compares with 40% and 80% to return the battery recharge power $P_{recharge,battery}^*$.

When SOC of the battery is lower than 80% and higher than 40%, the battery is under normal operating range. The output of the S-R Flip Flop is zero, which makes the battery recharge power to zero, and in this case, the battery can feed the loads in the system in demand.

When SOC of the battery is lower than 40%, the battery is under abnormal operation state, and the battery needs to be recharged immediately. The output of the S-R Flip Flop is one, which makes the battery recharge power to the negative of rated battery power $-25kW$. The battery recharge power will be used as an input for the power management subsystem.

6.2 Power Management Subsystem

The power management system shown in Figure 6.2 controls the reference power of the electrical motor by splitting the power demand as a function of the available power of the battery and the generator. The required generator power is achieved by controlling the generator torque, the motor torque and the battery recharge power.

The EMS ensures that required motor power never exceeds available power. Depending on the speed changes curve and Table 6.1, the required drive power (P_{drive}) was calculated. The required generator power (P_{gen}) was obtained by subtracting the battery recharge power ($P_{recharge}$) from P_{drive} . A look-up table based on the polarization curve was used to calculate required generator torque.

$$P_{Gen}^* = P_{drive}^* - P_{recharge,battery}^*$$

Table 6.1 Speed vs. Torque for Motor to calculate P_drive

Speed(rpm)	0	1200	2000	3000	4000	5000	6000
Torque	400	400	280	222.8169	179.0493	143.2394	119.3662

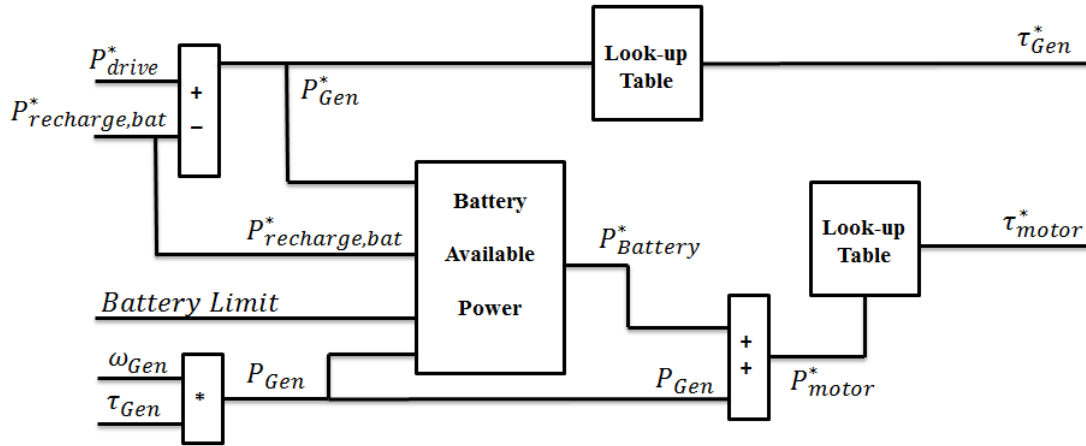


Figure 6.2 Power Management Subsystem

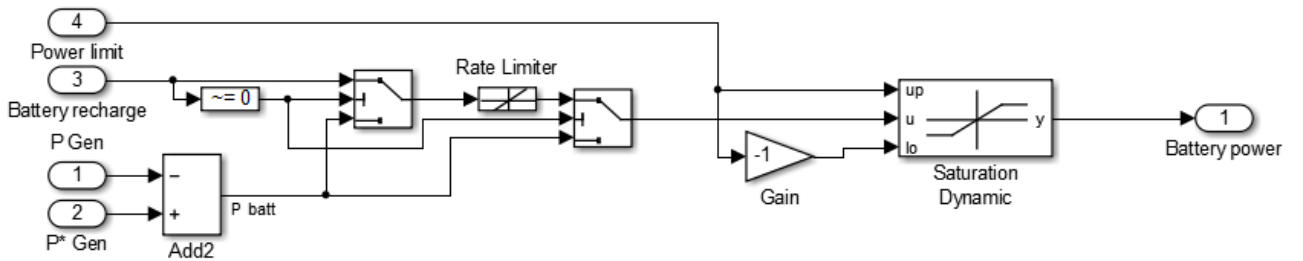


Figure 6.3 Battery Available Power Subsystem

Because the generator response time is large, the required generator power cannot be obtained instantaneously. The required motor power (P_{motor}) is limited by total available power (measured generator power and battery required power) in order to prevent a bus voltage collapse. Required battery power (P_{batt}) is obtained by subtracting required generator power P_{gen} from measured generator power (P_{gen}) shown in Figure 6.3. Depending on battery SOC and maximum power, the required battery power is also limited.

$$P_{\text{Battery}}^* = P_{\text{Gen}}^* - P_{\text{Gen}}$$

$$P_{\text{motor}}^* = P_{\text{Battery}}^* + P_{\text{Gen}}$$

The SPS is simulated during 16 s and covers three different operation modes: acceleration, cruising, and deceleration.

EMS improvement and component evaluation of the design parameters were obtained through simulation trial. For example, to avoid exceeding maximum battery power, the electric motor can be directly controlled to limit its torque. Therefore, the simulation using the battery model allows analysis of this complex phenomenon. Moreover, this EMS model helps develop the SPS, which controls all converters and the generator, to avoid exceeding maximum available power. Finally, the charge and discharge of the battery can be precisely controlled. This model, therefore, is the central point of SPS components.

6.3 Summary

This chapter presents a torque-controlled Energy Management System for the shipboard power system with backup battery pack. The EMS determines the reference torque signals for the

electric motor drives, the electric generator drive in order to distribute accurately the power from the two electrical sources. The control of the state of charge of battery pack is also concluded in this system to keep the battery from overcharging or undercharging.

Chapter 7 - Performance and Testing of the Developed Models

The next step in the process is to test the models. Disconnected with energy storage devices, the stability of the shipboard power system will be tested first. The performance of energy management system will be tested later with integration of shipboard power system, battery model and bidirectional DC/DC converter.

7.1 Stability of Shipboard Power System

As discussed in Chapter 3, in this system, each generator feeds one of the DC bus. From each bus, a buck converter feeds each load in a redundant way so that the load can be fed from the other bus if power fails on one bus.

Figure 7.1 displays the zone voltages in case of a starboard busfault. The generator on the starboard bus was shutted down. The fault is set at time 0.5 s with duration of 0.1 s as shown in Figure 7.1. Reviewing the loads scope through even there is a fault; this does not affect the loads' response, because it is fed from the second bus. This real time simulation ran on a dual-Xeon-based, 2.33 GHz and RT-LAB simulator with a time step of 35 microseconds. The processors allocation and real-time performance are summarized in Table 7.1.

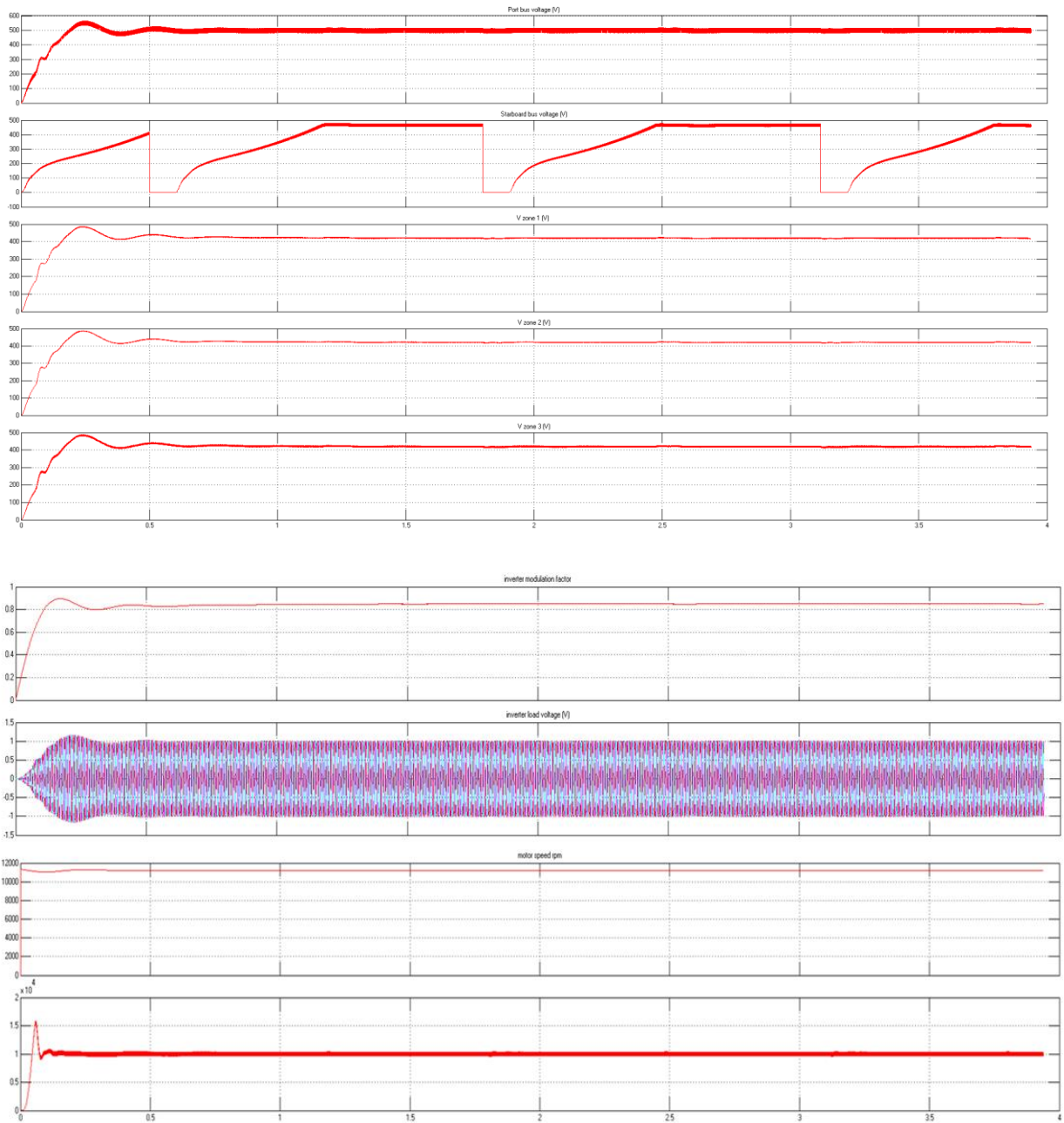


Figure 7.1 Simulation results in case of a Starboard Fault

Table 7.1 Processor Allocation and Real-Time Performance in case of a Starboard Fault

Descriptions CPUs	Components Content	Model Calculation Time	Minimum Time Step	Acceleration Factor
CPU 1:(35 us)	Generation	11 us	31 us	20 us
CPU 2:(35 us)	Loads	12 us		

7.2 Energy Management System Performance

The following result show different operating modes of the shipboard power system over one complete cycle: accelerating, cruising, recharging the battery while accelerating and regenerative braking. The all simulation lasts 16 s. These results were obtained by maintaining the accelerator constant to 70% for the first 4 s, and to 25% for the next 4 s, then to 85% when the speed increased again for 4 s and finally sets to -70% (braking) until the end of the simulation. The following explains what happens in Figure 7.3-7.7 when the shipboard power system is operating:

- At $t = 0$ s, the shipboard power system stopped and the speed increased to 70 %. Since the generator was unable to start as quickly as required, the battery provided motor power until the generator started.
- At $t = 0.3$ s, the generator began to provide power but it was unable to reach the reference power. Therefore, the battery continued to provide electrical power to the motor.
- At $t = 4$ s, the speed was released to 25%. The generator could not decrease its power instantaneously; therefore, the battery absorbed excess drive power in order to maintain required power.

- At $t = 8$ s, the speed was pushed to 85%. The battery helped the generator by providing an extra 20 kW of power.
- At $t = 11$ s, the battery SOC became lower than 40% (initialized to 40.5 % at the beginning of the simulation); therefore, the battery needed to be recharged. The generator shared power between the battery and motor. The battery power became negative, meaning that the battery received some power from the generator and recharged while the SPS accelerated. At this moment, required torque could no longer be met.
- At $t = 13$ s, the speed changes is set to -70% (regenerative braking is simulated). This is done by switching off the generator (the generator power takes 0.5 s to decrease to zero) and by ordering the motor to act as a generator. The kinetic energy of the SPS is transformed as electrical energy which is stored in the battery.
- At $t = 13.5$ s, the generator power is completely stopped

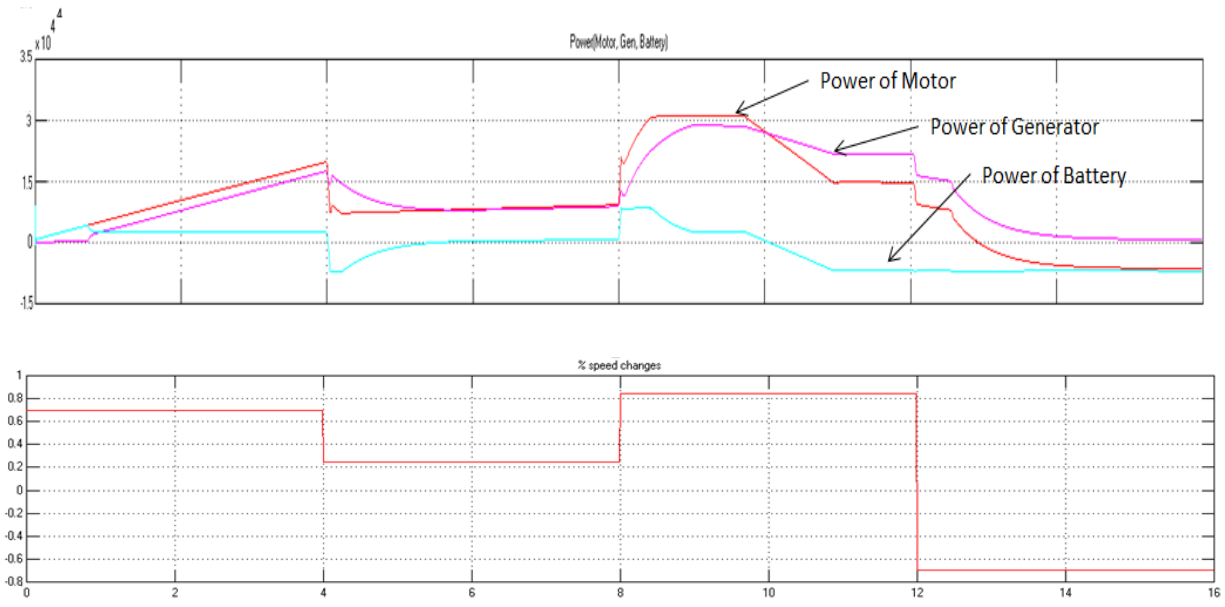


Figure 7.2 Simulation results of acceleration factor, and power of generator, motor and battery

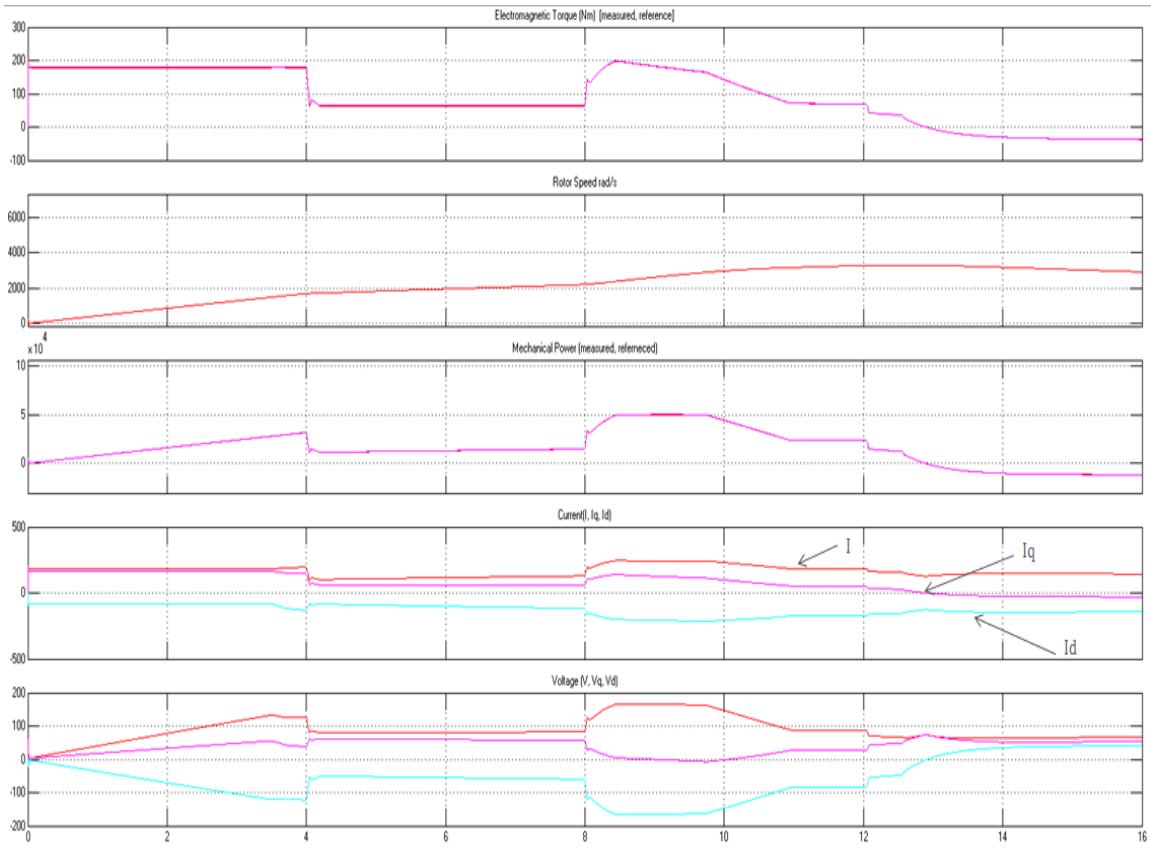


Figure 7.3 Simulation results of PMSM motor drive parameters

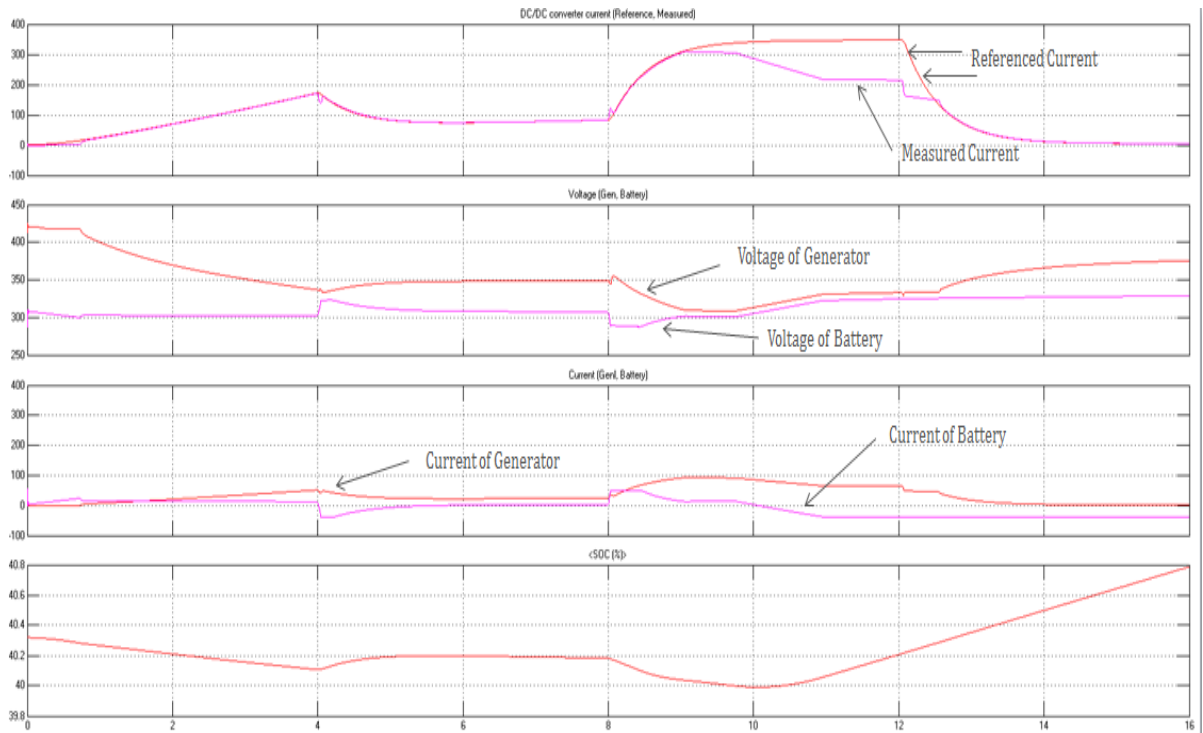


Figure 7.4 Simulation results of SOC, voltage and current of battery, and voltage and current of generator and DC-DC converter

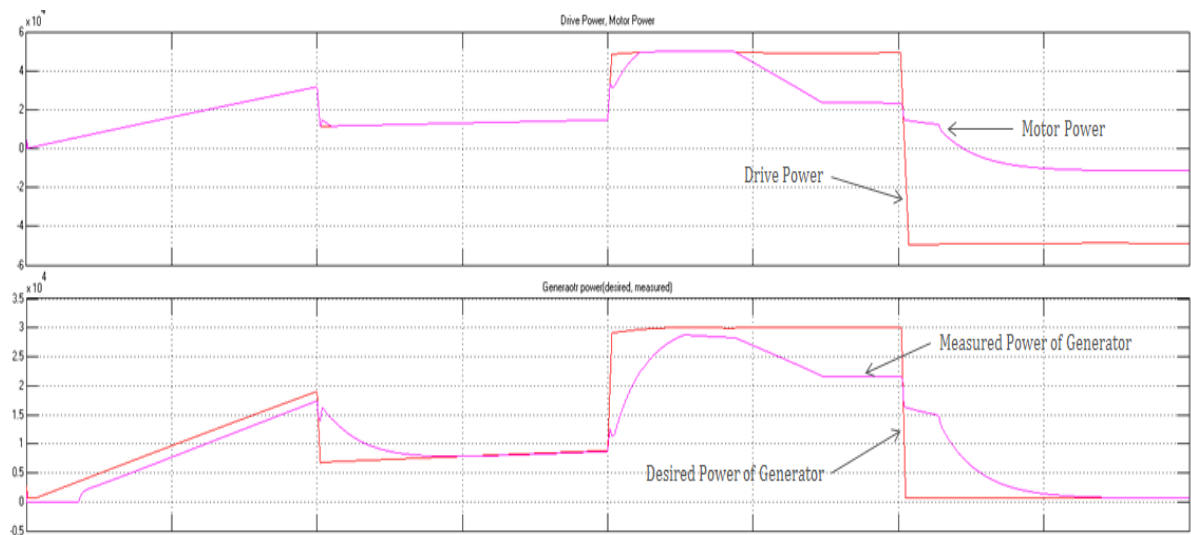


Figure 7.5 Simulation results of drive power, motor power, battery power and generator power

Chapter 8 - Discussion and Future Work

The Energy Management System can control the power flow between shipboard power system and energy storage devices under steady-state (normal) mode, acceleration mode and braking (regenerative) mode and can increase stability and sustainability of shipboard power system. The shipboard power system performs well in those three modes. During acceleration mode, power flow travels from battery to power system where, similar to regenerative mode, kinetic energy of the motor is converted into electrical energy and fed back to the battery. In addition, generators inside the shipboard power system can charge battery packs under normal mode when the State-Of-Charge (SOC) level of battery packs is below the standard level. The survivability of the shipboard power system is also demonstrated. By using each generator feeds each bus in a redundant way, the stability of power system is highly increased. Also, the bidirectional DC/DC converter allows the power flow between the power system and the battery.

The energy management system and bidirectional DC-DC converter designed in this thesis are also suitable for the power control and integration of other electric systems with backup energy storage devices. The diagram of power train by using energy management system and bidirectional DC-DC converter for electric systems is shown in Figure 8.1.

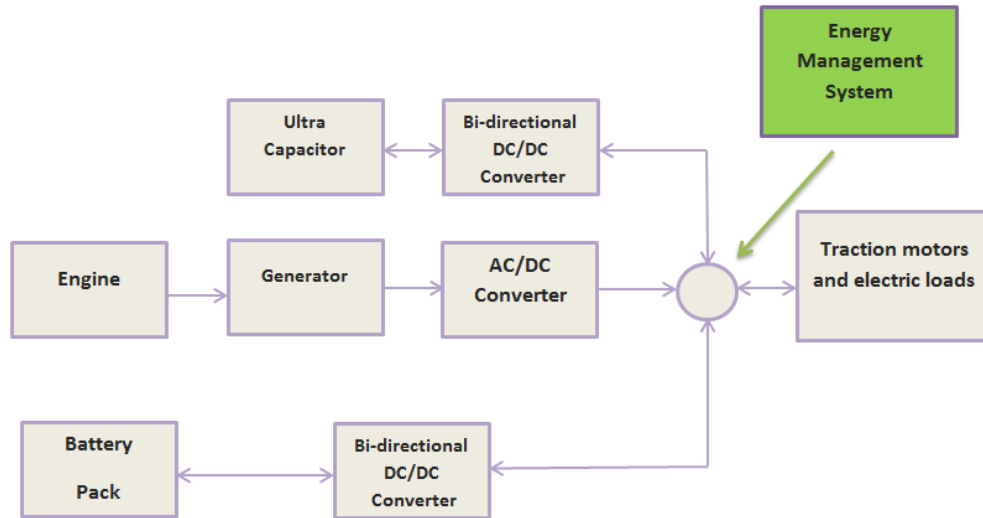


Figure 8.1 Diagram of powertrain using designed model

In this research, several previous research results were extended to include the integration of the shipboard power system and battery storage. Models were modified and implemented for the battery, bidirectional DC-DC converter and shipboard power system. These models were combined to demonstrate the various models in different system states.

The performance of various ESD combinations, including ultracapacitors at different fault locations can be tested and evaluated in future work to decide the best combination of ESD size, type, and location. Utilization of the system developed in my research will allow future tests to be conducted, such as building sensors to locate faults, testing relay performance, and investigating the tolerance of system parameters.

References

- [1] Dieker. Joseph, “High impedance fault identification using Bayesian analysis in a shipboard power system”, MS. Thesis Kansas State University. 2012-09-06T14:28:30Z, September 2012. <http://krex.k-state.edu/dspace/handle/2097/14643>

- [2] Dufour, C., Andrade, C. and Bédanger, J., Real-Time Simulation Technologies in Education: a Link to Modern Engineering Methods and Practices. Retrieved March 3, 2012, from: <http://www.opal-rt.com/technical-document/real-time-simulation-technologies-education-link-modernengineering-methods-and>

- [3] Bédanger, J., Venne, P., and Paquin, J. The What, Where and Why of Real-Time Simulation. Retrieved March 9, 2012, from: http://www.opal-rt.com/sites/default/files/technical_papers/PESGM-Tutorial_04%20-%20Real%20Time%20Simulation.pdf

- [4] Banks, J., Carson, J., Nelson, B. & Nicol D. Discrete-Event System Simulation. (3rd ed.). Prentice Hall. (2001).

- [5] RT-Lab Quick Guide. Retrieved March 15, 2012, from: http://www.opal-rt.com/sites/default/files/RT-LAB_Quickstart.pdf

- [6] Artemis Guide. Retrieved March 15, 2012, from: [http://www.opal-rt.com/sites/default/files/ARTEMIS_User_Guide\(1\).pdf](http://www.opal-rt.com/sites/default/files/ARTEMIS_User_Guide(1).pdf)

- [7] RT-Event Guide. Retrieved March 15, 2012, from: [http://www.opal-rt.com/sites/default/files/RTEVENTS_User_Guide\(1\).pdf](http://www.opal-rt.com/sites/default/files/RTEVENTS_User_Guide(1).pdf)

- [8] Kesete. Amanuel, “Optimization of storage integrations into MVDC in shipboard power system”, Master Report Kansas State University. May 2012.

- [9] Kroeze, R. C, “Electrical battery model for use in dynamic electric vehicle simulations”, University of Illinois at Urbana-Campaign, Tech. Rep. UILU-ENG-98-0409, December 1998.

- [10] Kumar, A.A., “Technical and economic impacts of distributed generators and energy storage devices on the electric grid”, Mississippi State University, December 2008.
- [11] Barrade, P., “Energy storage and applications with supercapacitors”, *Paper presented at the National Association of Electric Drives, 14th Seminar on Electric drives: trends and issues*, Bressanone, Italy, March 2003.
- [12] Hirachi, K., M. Yamanaka, K. Kajiyama and S. Isokane, “Circuit Configuration of Bidirectional DC/DC Converter Specific for Small Scale Load Leveling System,” *IEEE Transactions on Power Conversion*, Vol. 2, 2002, pp. 603-609.
- [13] Jain, P.K., Kang, W., Soin, H., and Xi Y., Analysis and design consideration of a load and line independent Zero voltage switching Full bridge DC/DC Converter topology, *IEEE Transactions on Power Electronics*, Vol.17, No.5, September. Pp 649-657. 2002
- [14] Rahmani, S. , K. Al-Haddad and H. Y. Kanaan, “Two PWM Techniques for Single-Phase Shunt Active Power Filters Employing a Direct Current Control Strategy,” *IET Power Electron*, Vol. 1, No. 3, 2008, pp. 376-385. doi:10.1049/iet-pel:20070253
- [15] Zhang Y., and Sen P.C. A new soft switching technique for buck, boost, and buck-boost converters, *IEEE transactions on Industry Applications*, Vol. 39. No.6, November/December, pp. 1775-1782. , 2003.

Appendix A - Parameters of Battery

C_SOC_Ctrans_m	C_C_Ctrans_m
0	19.02
0.05396	1490.1
0.10793	2163.64
0.16189	1722.67
0.21586	1854.73
0.26982	2294.37
0.32379	1532.73
0.37775	1420.86
0.43172	1877.63
0.48568	1787.58
0.53965	3296.25
0.59361	3967.54
0.64758	1319.42
0.70154	1138.83
0.75551	972.1
0.80947	1063.35
0.86344	1287.51
0.9174	1244.14
0.97497	1008.46
1	1195.42

C_SOC_Ctrans_s	C_C_Ctrans_s
0	0.74713
0.05396	2.16892
0.10793	1.41609
0.16189	1.37996
0.21586	1.76225
0.26982	1.007
0.32379	1.24868
0.37775	0.65976
0.43172	0.93241
0.48568	0.87565
0.53965	0.57543
0.59361	0.86314
0.64758	0.73236
0.70154	0.89511
0.75551	1.29471

0.80947	0.83917
0.86344	0.71082
0.9174	1.31685
0.97497	0.8056
1	0.71929
C_SOC_Rseries	C_R_Rseries
0	0.047666
0.05396	0.067527
0.10793	0.057597
0.16189	0.063555
0.21586	0.065541
0.26982	0.051639
0.32379	0.063555
0.37775	0.049652
0.43172	0.055611
0.48568	0.057597
0.53965	0.047666
0.59361	0.057597
0.64758	0.047666
0.70154	0.055611
0.75551	0.059583
0.80947	0.051639
0.86344	0.055611
0.9174	0.065541
0.97497	0.055611
1	0.057597

C_SOC_Rtrans_m	C_R_Rtrans_m
0	1.78139
0.05396	0.0436
0.10793	0.02774
0.16189	0.04486
0.21586	0.04282
0.26982	0.03272
0.32379	0.03592
0.37775	0.03869
0.43172	0.03614
0.48568	0.05035
0.53965	0.05008

0.59361	0.04916
0.64758	0.04164
0.70154	0.03651
0.75551	0.04113
0.80947	0.04235
0.86344	0.04267
0.9174	0.05633
0.97497	0.0645
1	0.05443

C_IRF	C_RF
0	1
0.0808	1
0.4389	1.00542
1.0886	1.03632
2.1603	1.08318

D_SOC_Ctrans_h	D_C_Ctrans_h	C_C_Ctrans_h
0	370000	370000
0.25	6500000	6500000
0.5	563000	563000
0.75	3440000	3440000
1	2240000	2240000

D_SOC_Ctrans_m	D_C_Ctrans_m
0	19.02
0.07662	1239.63
0.17877	1289.33
0.19535	1716.31
0.27233	4780.89
0.36655	3799.46
0.43889	7430.52
0.4999	1639.71
0.54379	1402.43
0.59429	1230.37
0.63879	2384.93
0.74914	2781.03
0.79836	2146.55
0.85892	1230.39
0.91208	976.47
0.96788	1441.14
1	1195.42

D_SOC_Ctrans_s	D_C_Ctrans_s		
0	0.68968		
0.07662	1.36985		
0.17877	1.9824		
0.19535	1.2384		
0.27233	1.204		
0.36655	1.512		
0.43889	1.43071		
0.4999	1.2096		
0.54379	0.96768		
0.59429	0.73662		
0.63879	0.966		
0.74914	0.88704		
0.79836	0.77891		
0.85892	0.88941		
0.91208	0.936		
0.96788	0.94871		
1	0.756		
D_SOC_Rseries	D_R_Rseries		
0	0.047619		
0.07662	0.05754		
0.17877	0.06746		
0.19535	0.059524		
0.27233	0.055556		
0.36655	0.065476		
0.43889	0.061508		
0.4999	0.059524		
0.54379	0.055556		
0.59429	0.053571		
0.63879	0.05754		
0.74914	0.05754		
0.79836	0.053571		
0.85892	0.053571		
0.91208	0.05754		
0.96788	0.053571		
1	0.051587		
D_SOC_Rtrans_h	D_R_Rtrans_h	C_R_Rtrans_h	
0	0.027	0.027	
0.25	0.002	0.002	
0.5	0.00408	0.00408	
0.75	0.00189	0.00189	

1		0.00357	0.00357
D_SOC_Rtrans_m	D_R_Rtrans_m		
0	1.78139		
0.07662	0.07974		
0.17877	0.04188		
0.19535	0.02851		
0.27233	0.03556		
0.36655	0.03394		
0.43889	0.0288		
0.4999	0.039		
0.54379	0.03494		
0.59429	0.0357		
0.63879	0.04717		
0.74914	0.04851		
0.79836	0.04202		
0.85892	0.04212		
0.91208	0.03988		
0.96788	0.02992		
1	0.05443		

Appendix B - Figures

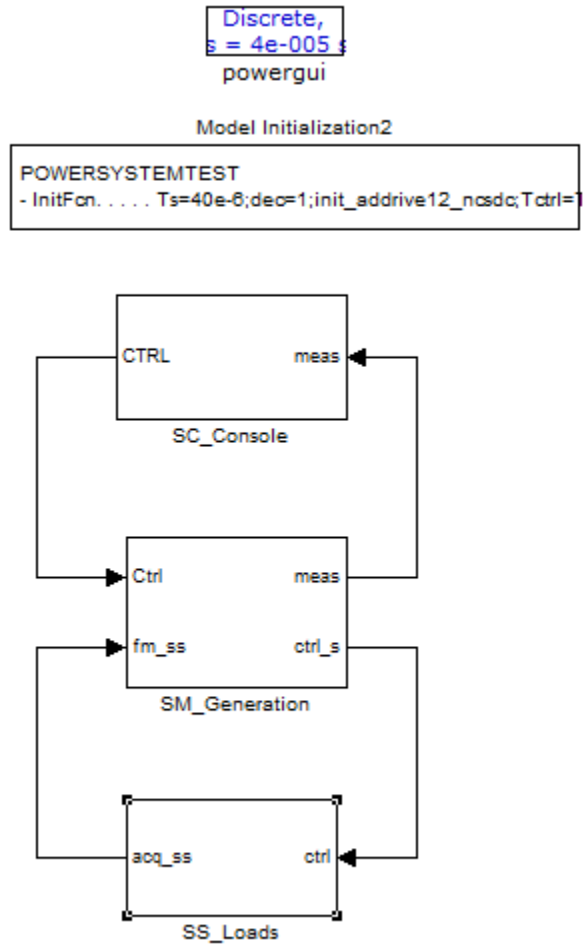


Figure 1 – Whole system in RT-Lab

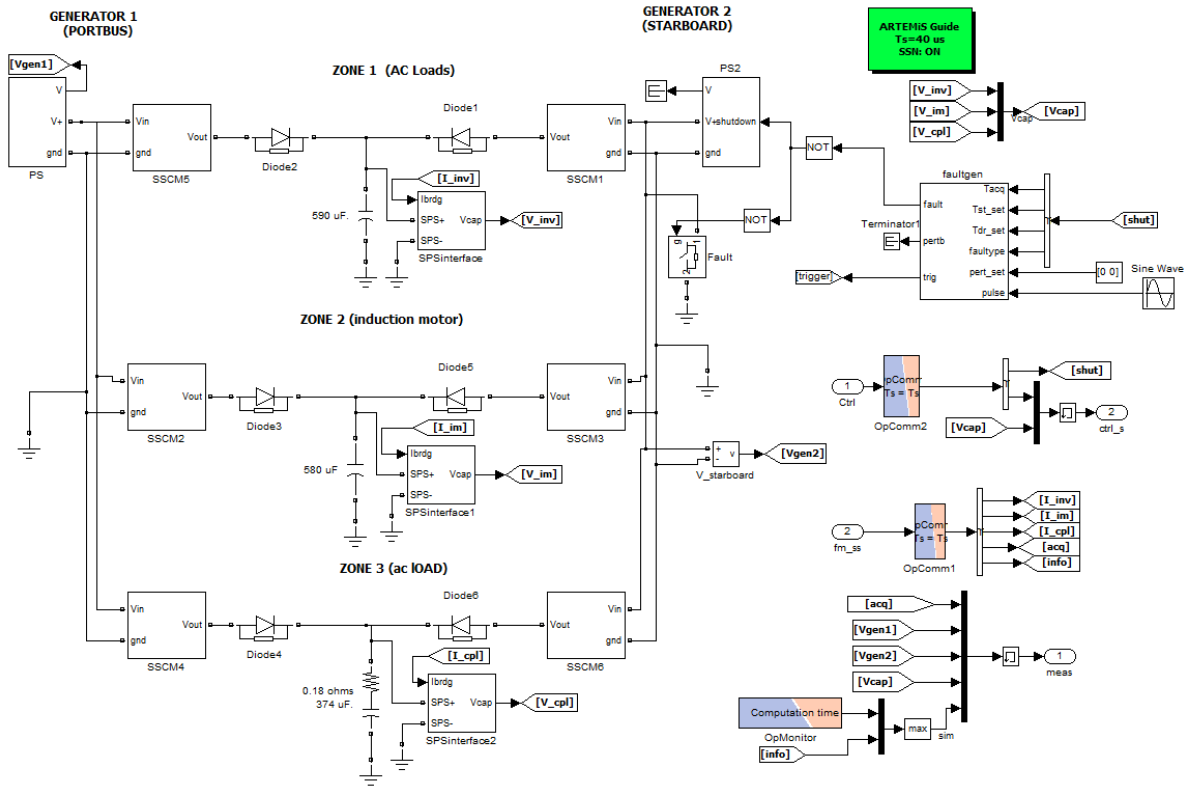


Figure 2 – Generation Part of system

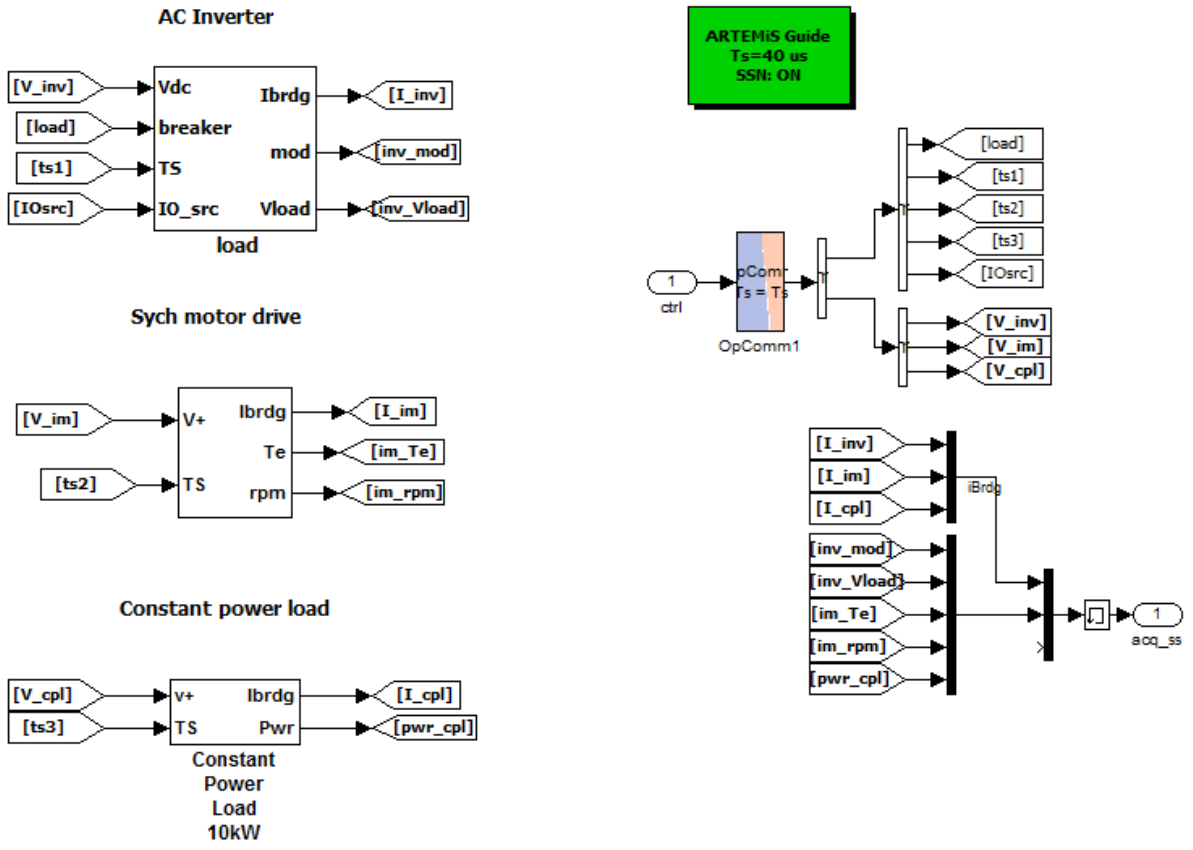


Figure 3 – Load Zones

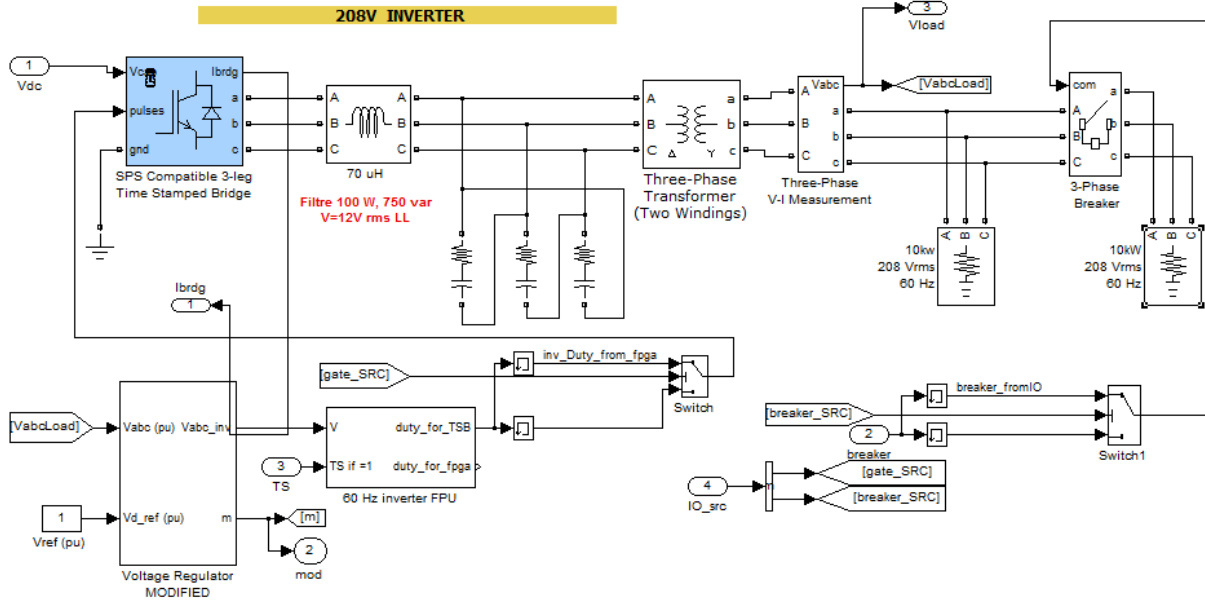


Figure 4 – Ac Load Zone

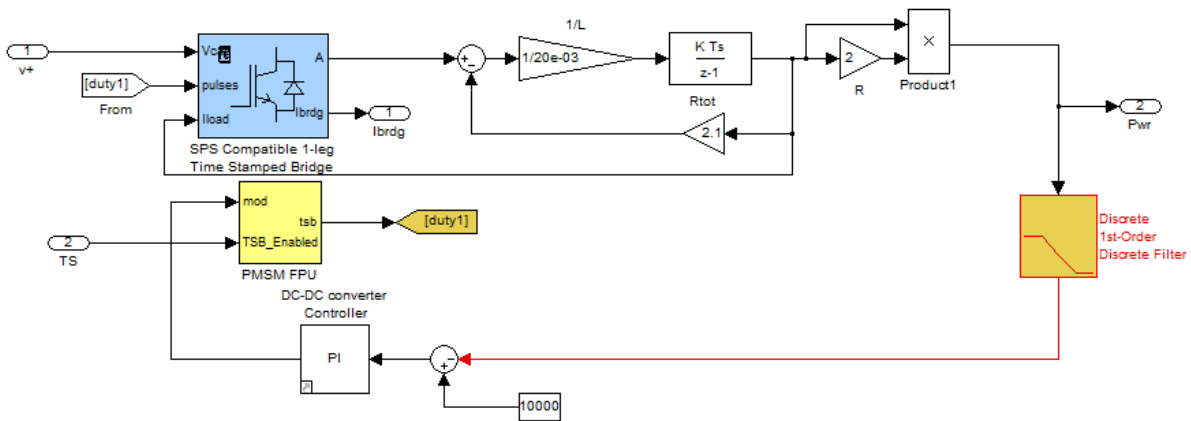


Figure 5 – Constant Power Zone

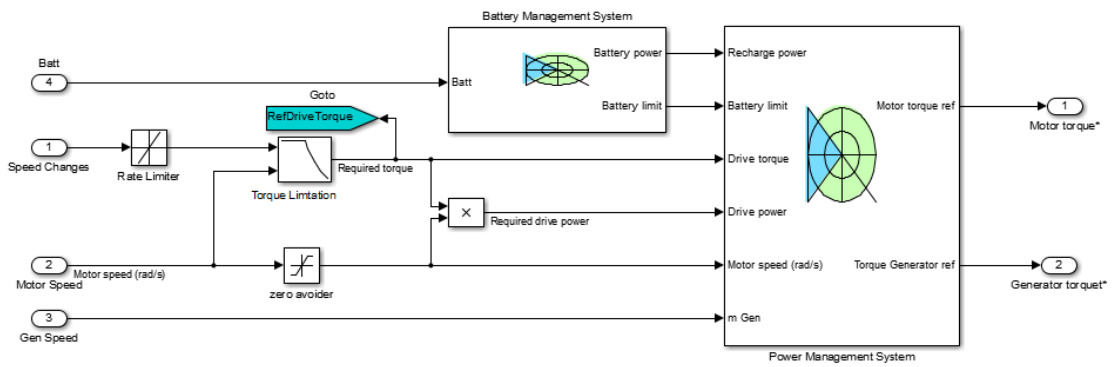


Figure 6 – Energy Management System

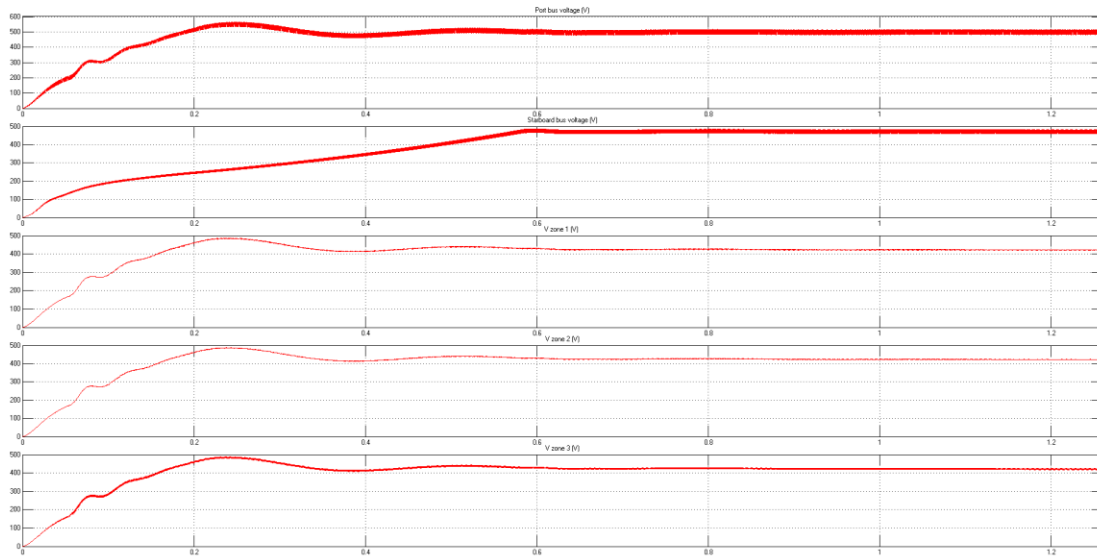


Figure 7 – Bus Voltages without Fault

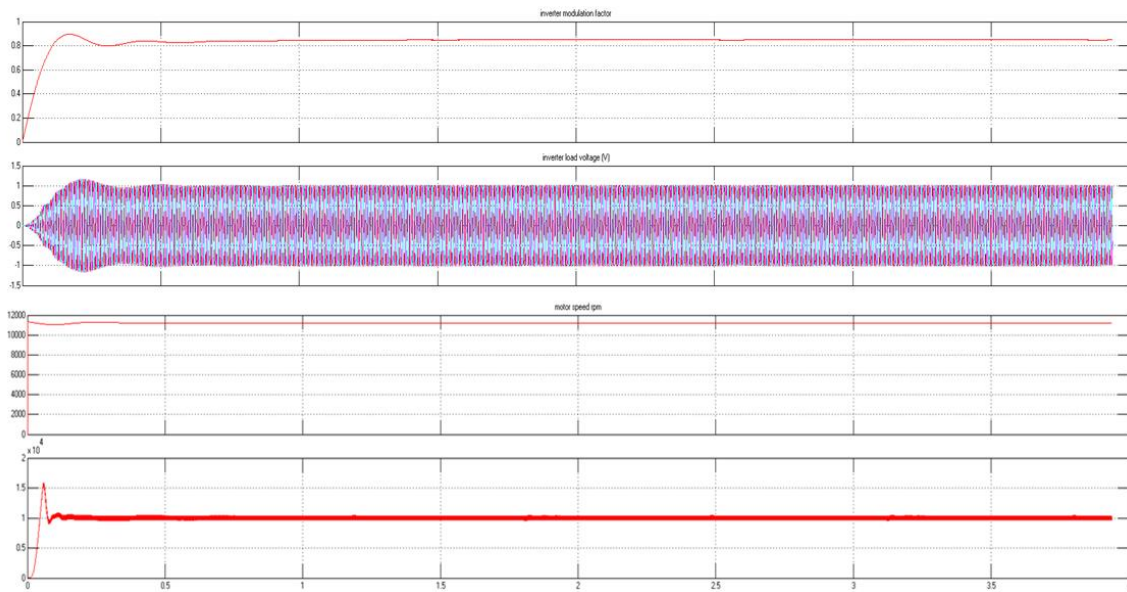


Figure 8 – Load Zones

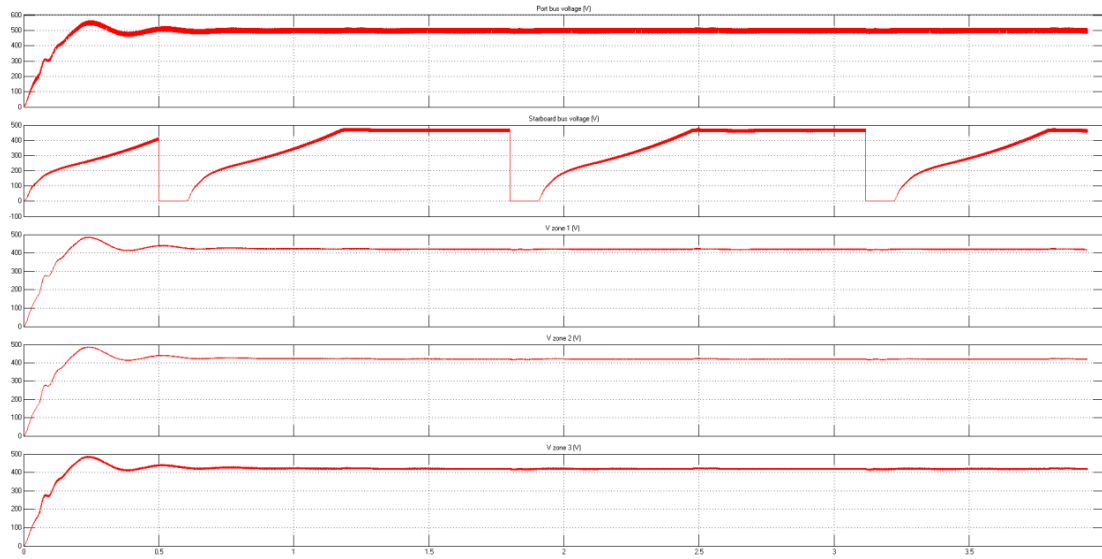


Figure 9 – Starboard Fault Simulation

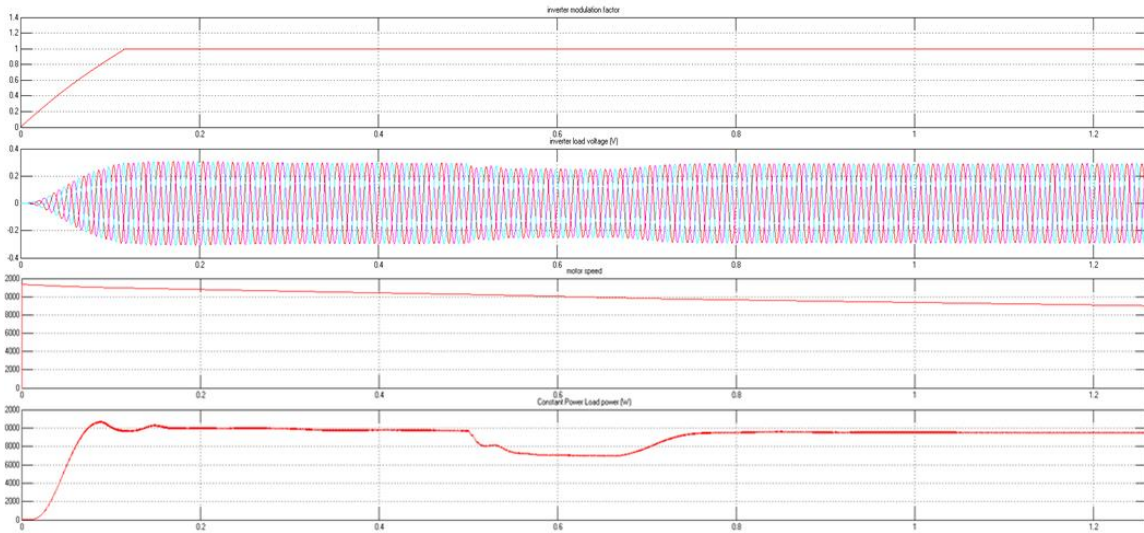


Figure 10 – Load Zones Response to the Fault

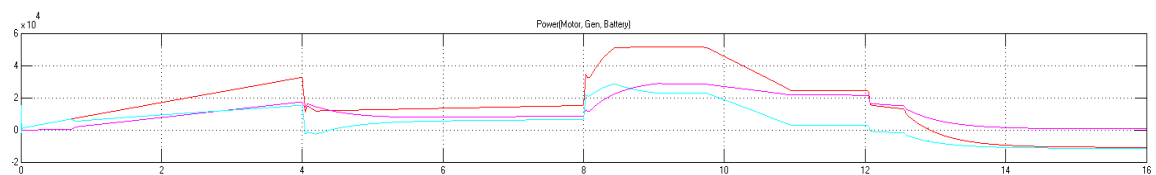


Figure 11-Simulation results of acceleration factor, and power of generator, motor and battery

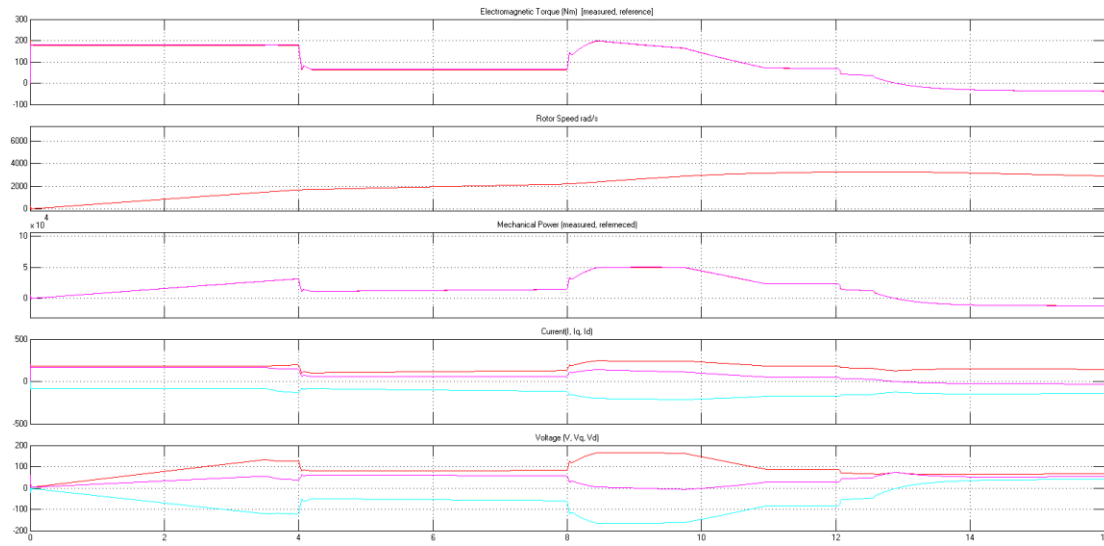


Figure 12- Simulation results of PMSM motor drive parameters

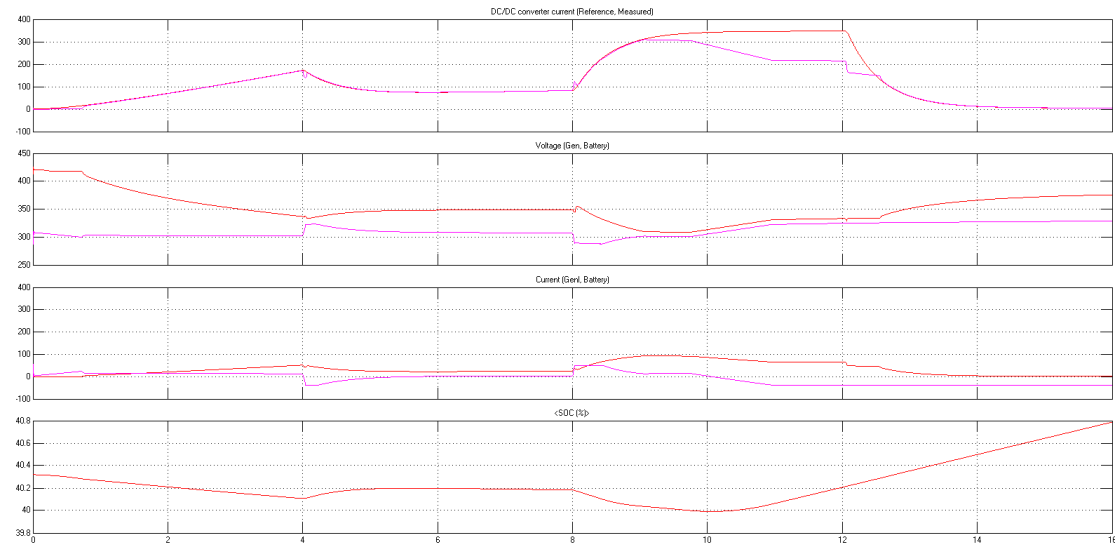


Figure 13- Simulation results of SOC, voltage and current of battery, and voltage and current of generator and DC-DC converter

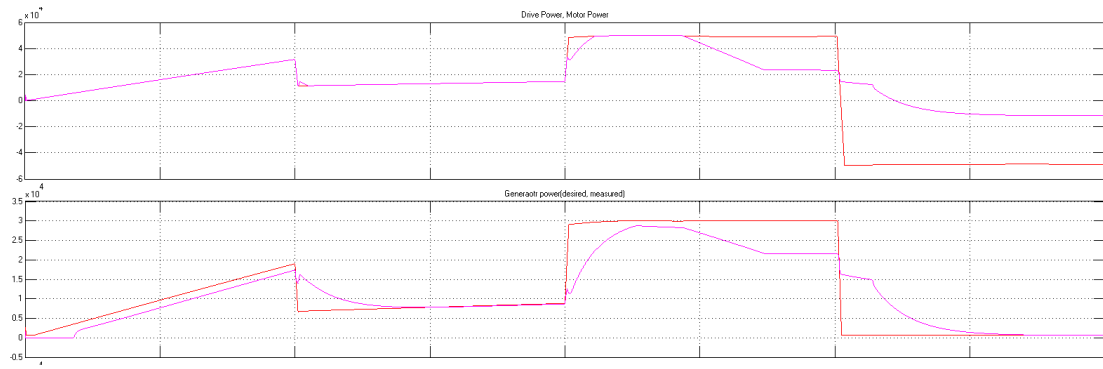


Figure 14- Simulation results of drive power, motor power, battery power and generator power